Synthesis and Characterization of Organohydrazino Complexes of Technetium, Rhenium, and Molybdenum with the $\{M(\eta^1\text{-}H_xNNR)(\eta^2\text{-}H_yNNR)\}$ Core and Their Relationship to Radiolabeled Organohydrazine-Derivatized Chemotactic Peptides with Diagnostic Applications

David J. Rose,*,† Kevin P. Maresca,† Terrence Nicholson,‡ Alan Davison,‡ Alun G. Jones,§ John Babich,*,|| Alan Fischman,|| Wendy Graham,|| Jeffery R. D. DeBord,† and Jon Zubieta*,†

Department of Chemistry, Syracuse University, Syracuse, New York 13244, Chemistry Department, Massachusetts Institute of Technology, Cambridge, Massachusetts 02139, Department of Radiology, Harvard Medical School and Brigham and Women's Hospital, Boston, Massachusetts 02215, and Department of Radiology, Massachusetts General Hospital, Boston, Massachusetts 02214

Received March 27, 1997

The reduction of perrhenate, molybdate and pertechnetate with 2-hydrazinopyridine dihydrochloride in methanol has led to the preparation of a class of complexes containing the $\{M(\eta^1\text{-}NNC_5H_4NH_x)(\eta^2\text{-}HNNH_yC_5H_4N)\}$ core, represented by $[TcCl_3(NNC_5H_4NH)(HNNC_5H_4N)]$ (**2**), $[ReCl_3(NNC_5H_4NH)(HNNC_5H_4N)]$ (**3**), and $[MoCl_3(NNC_5H_4NH)(HNNHC_5H_4N)]$ (**6**). The reaction of **3** with NEt_3 results in the formation of $[HNEt_3][[ReCl_3(NNC_5H_4N)(HNNC_5H_4N)]\cdot H_2O$ (**4**) by deprotonation of the pyridine nitrogen site. Similarly, the reduction of perrhenate with 2-hydrazino-2-imidazoline hydrobromide has led to the preparation of the analogous $[ReCl_3(NNC_3H_4N_2H)(HNNHC_3H_4N_2H)]$ (**5**). Reaction of **3** with pyridine-2-thiol and pyrimidine-2-thiol yields two structurally characterized derivatives with a modified $\{Re(\eta^1\text{-}NNC_5H_4N)(\eta^2\text{-}HNNC_5H_4N)\}$ core, $[Re(C_5H_4NS)_2(NNC_5H_4N)(HNNC_5H_4N)]$ (**8**) and $[Re(C_4H_3N_2S)_2(NNC_5H_4N)(HNNC_5H_4N)]$ (**9**), respectively. Reaction of **6** with pyrimidine-2-thiol led to the isolation of the analogous $[Mo(C_4H_3N_2S)_2(NNC_5H_4N)(HNNHC_5H_4N)]$ (**11**) and the seven-coordinate monohydrazine core complex $[Mo(C_4H_3N_2S)_3(NNC_5H_4N)]\cdot CH_2Cl_2$ (**12**). In similar fashion, the reaction of **2** with pyridine-2-thiol yielded a complex structurally analogous to **8**, $[Tc(C_5H_4NS)_2(NNC_5H_4N)(HNNC_5H_4N)]$ (**7**). Crystal data for **3**, $C_{10}H_{10}Cl_3N_6Re$: triclinic, $P\bar{1}$, $a = 7.527(2)$ Å, $b = 7.599(2)$ Å, $c = 13.118(3)$ Å, $\alpha = 106.55(3)°$, $\beta = 90.28(3)°$, $\gamma = 93.83(3)°$, $V = 717.4(4)$ Å^3, $Z = 2$. For **4**, $C_{16}H_{27}Cl_3N_7ORe$: orthorhombic, $P2_12_12_1$, $a = 7.503(2)$ Å, $b = 10.3643(2)$ Å, $c = 30.1590(5)$ Å, $V = 2345.20(6)$ Å^3, $Z = 2$. For **5**, $C_6H_{12}Cl_3N_8Re$: monoclinic, $P2_1/n$, $a = 9.093(2)$ Å, $b = 11.105(2)$ Å, $c = 14.295(3)$ Å, $\beta = 94.71(3)°$, $V = 1438.6(7)$ Å^3, $Z = 4$. For **6**, $C_{10}H_{11}Cl_3N_6Mo$: monoclinic, $P2_1/c$, $a = 15.366(3)$ Å, $b = 7.804(2)$ Å, $c = 12.378(3)$ Å, $\beta = 95.92(3)°$, $V = 1476.4(5)$ Å^3, $Z = 4$. For **7**, $C_{20}H_{17}N_8S_2Tc$: monoclinic, $P2_1$, $a = 8.827(2)$ Å, $b = 9.278(2)$ Å, $c = 13.304(3)$ Å, $\beta = 98.92(3)°$, $V = 1076.5(5)$ Å^3, $Z = 2$, 2564 reflections. For **8**, $C_{20}H_{17}N_8S_2Re$: monoclinic, $P2_1$, $a = 8.848(2)$ Å, $b = 9.190(2)$ Å, $c = 13.293(3)$ Å, $\beta = 98.89(3)°$, $V = 1067.9(5)$ Å^3, $Z = 2$. For **9**, $C_{18}H_{15}N_{10}S_2Re$: monoclinic, $P2_1$, $a = 8.796(2)$ Å, $b = 9.008(2)$ Å, $c = 13.208(3)$ Å, $\beta = 97.90(3)°$, $V = 1036.6(5)$ Å^3, $Z = 2$. For **12**, $C_{18}H_{15}N_9S_3Cl_2Mo$: monoclinic, $P2_1/n$, $a = 10.52900(10)$ Å, $b = 15.1116(3)$ Å, $c = 15.8193(3)$ Å, $\beta = 108.4790(10)°$, $V = 2387.23(7)$ Å^3, $Z = 4$. Complexes **2** and **3** serve as models for the binding of Tc(V)−oxo and Re(V)−oxo species to hydrazinonicotinamide (HYNIC)-conjugated chemotactic peptides. Furthermore, since the use of the pyrimidinethiol coligand in the $\{^{99m}Tc$−HYNIC−peptide$\}$ radiochemical species results in favorable pharmacokinetics, the thiolate derivatives **8** and **9** provide models for possible modes of interaction of metal−hydrazine cores with coligands in the radiopharmaceutical reagents.

Introduction

Radioisotopes conjugated to proteins provide a means for imaging and treatment of disease. We have demonstrated that bifunctional hydrazine ligands function as effective and versatile linkers for labeling antibodies and protein fragments.[1] Specifically, when *N*-oxysuccinimidylhydrazinonicotinamide (**1**) is combined with a macromolecule such as a protein, polypeptide, or glycoprotein in neutral or slightly basic media, the protein-reactive part of the compound reacts with nucleophilic groups in the macromolecule, such as the amine groups of lysine residues, to yield a conjugate containing free hydrazine/hydrazide groups, referred to as HYNIC−protein (Scheme 1).

The hydrazine unit acts as an effective ligating group for metal cations[2] which are incorporated into the conjugate to yield the labeled macromolecule. The versatility of the linker technology in related applications, such as the synthesis of conjugates of chemotactic peptides, has led to natural products which bind to high-affinity receptors on white blood cell membranes and thereby migrate to sites of infection.[3] The advantages of this type of molecule over antibodies include smaller size and enhanced diffusibility to the extravascular space, faster blood clearance resulting in lower background

† Syracuse University.
‡ MIT.
§ Harvard Medical School.
|| Massachusetts General Hospital.

S0020-1669(97)00352-2 CCC: $15.00
Published on Web 05/08/1998

Scheme 1. Derivatization and Labeling of a Protein with HYNIC (**1**) and Radioisotope M

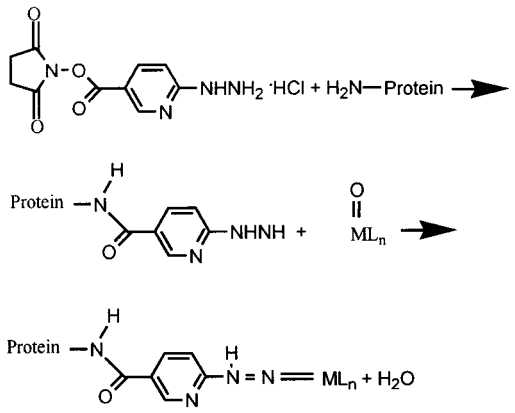

radiation, the presence of well-defined receptor systems, and the ability to synthesize analogues of these peptides with varying size, charge, and linker properties.[4] In fact, ^{99m}Tc-labeled hydrazinonicotinamide chemotactic peptides have now been shown to be effective agents for rapid detection of focal sites of infection in animals.[5] Furthermore, radiolabeling of such peptides with β-emitting isotopes such as ^{188}Re, a congener of Tc, shows some promise for the development of therapeutic reagents with biodistributions similar to those of the diagnostic ^{99m}Tc reagents.[6]

As shown in Scheme 2, labeling of the HYNIC−peptide via a ^{99m}Tc(V)−oxo species is effected by reduction of a $^{99m}TcO_4^-$ solution with a solution of $SnCl_2$ in aqueous mannitol, addition of the HYNIC-conjugated peptide, and subsequent purification by HPLC to give the radiolabeled {^{99m}Tc−(mannitol)−HYNIC−peptide}. It is noteworthy that the choice of coligand has a profound effect on the organ distribution of the labeled peptide. In infected rabbits HYNIC-conjugated chemotactic peptides labeled via ^{99m}Tc-mannitol gave superior imaging results as compared with other polyhydridic "coligands". However, radio-HPLC indicated the presence of several ^{99m}Tc−peptide species, a likely result of the presence of {Tc−(coligand)−HYNIC−peptide} isomers.[7]

Scheme 2. Labeling of the HYNIC−peptide via a Tin(II)-Reduced ^{99m}Tc(V) Oxo Species and Subsequent Reaction with Pyrimidine-2-thiol

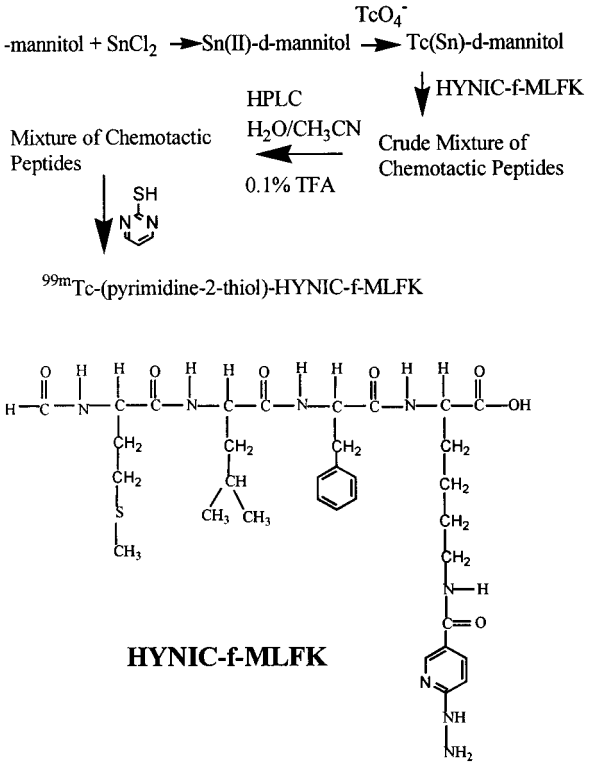

Scheme 3. The Thiolate Ligands of this Study

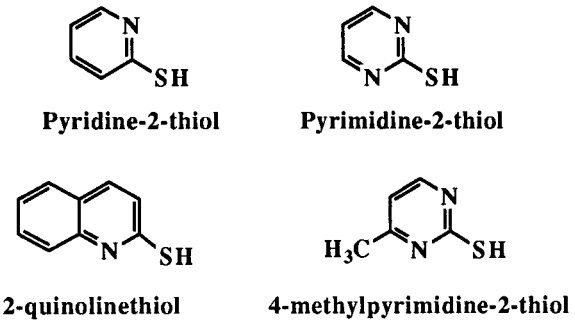

In order to formulate and mechanistic studies of ^{99m}Tc−HYNIC−peptide radiochemical species require homogeneous materials with favorable pharmacokinetics, the synthesis of high-purity compositions required some attention. To this end, an initial investigation of selected pyrimidinethiol and pyridinethiol coligands has been carried out. The thiols pyrimidine-2-thiol, 4-methylpyrimidine-2-thiol, pyridine-2-thiol, and 2-quinolinethiol, shown in Scheme 3, were reacted with {^{99m}Tc−(mannitol)−HYNIC−f-MLFK}, and the resultant ^{99m}Tc-labeled pyrimidinethiol and pyridinethiol peptide complexes were characterized by RP-HPLC. The {^{99m}Tc−(pyrimidine-2-thiol)−HYNIC−peptide} complex, hereafter denoted {^{99m}Tc(PmT)−HP}, was evaluated in a rabbit model of infection.

(1) (a) Schwartz, D. A.; Abrams, M. J.; Hauser, M. M.; Gaul, F. E.; Larsen, S. K.; Rauth, D.; Zubieta, J. A. *Bioconjugate Chem.* **1991**, *2*, 333−336. (b) Abrams, M. J.; Schwatrz, D. A.; Hauser, M. M.; Gaul, F. E.; Zubieta, J. A.; Larsen, S. K.; Fuccello, A. J. Riexinger, D. J. Jester, D. W. Presented at the 37th Meeting of the Society of Nuclear Medicine, Washington, DC, June 19−22, 1990. (c) Claessens, R. A.; Koenders, E. B.; Oyen, W. J. G.; Corstens, F. H. *Eur. J. Nucl. Med.* **1996**, *23*, 1536−9. (d) Lei, K.; Rusckowski, M.; Chang, F.; Qu, T.; Mardirossian, G.; Hnatowich, D. J. *Nucl. Med. Biol.* **1996**, *23*, 917−922. (e) Claessens, R. A.; Boerman, O. C.; Koenders, E. B.; Oyen, W. J.; van der Meer, J. W.; Corstens, F. H. *Eur. J. Nucl. Med.* **1996**, *23*, 414−421. (f) Liu, S.; Edwards, D. S.; Looby, R. J.; Harris, A. R.; Poirier, M. J.; Barrett, J. A.; Heminway, S. J.; Carroll, T. R. *Bioconjugate Chem.* **1996**, *7*, 63−71. (g) Hnatowich, D. J.; Mardirossian, G.; Fogarasi, M.; Sano, T.; Smith, C. L.; Cantor, C. R.; Rusckowski, M.; Winnard, P., Jr. *J. Pharm. Exp. Ther.* **1996**, *276*, 326−334. (h) Hnatowich, D. J.; Winnard, P., Jr.; Virzi, F.; Fogarasi, M.; Sano, T.; Smith, C. L.; Cantor, C. R.; Rusckowski, M. *J. Nucl. Med.* **1995**, *36*, 2306−2314. (i) Verbeke, K.; Hjelstuen, O.; Debrock, E.; Cleynhens, B.; De Roo, M.; Verbruggen A. *Nucl. Med. Comm.* **1995**, *16*, 942−57.

(2) (a) Bishop, M. W.; Chatt, J.; Dilworth, J. R.; Hursthouse, M. R.; Motevalli, J. *J. Chem. Soc.* **1979**, 1600. (b) Abrams, M. S.; Larsen, S. K.; Zubieta, J. A. *Inorg. Chem.* **1991**, *30*, 2031−2035. (c) Nicholson, T.; Davison, A. *Inorg. Chim. Acta* **1990**, *168*, 227. (d) Abrams, M. J.; Shaikh, S. N.; Zubieta, J. *Inorg. Chim. Acta* **1990**, *173*, 133.

(3) Hugli, T. E. *Curr. Opin. Immunol.* **1989**, *2*, 19.

(4) Fischman, A. J.; Pike, M. C.; Kroon, D.; Fucello, A. J.; Rexinger, D.; ten Kate, C.; Wilkson, R.; Rubin, R. H.; Strauss, H. W. *J. Nucl. Med.* **1991**, *32*, 483.

(5) (a) Babich, J. W.; Graham, W.; Barrow, S. A.; Fischman, A. J. *Nucl. Med. Biol.* **1995**, *22*, 643. (b) Babich, J. W.; Fischman, A. J. *Nucl. Med. Biol.* **1995**, *22*, 25. (c) Babich, J. W.; Solomon, H.; Pike, M. C.; Kroon, D.; Graham, W.; Abrams, M. J.; Tompkins, R. G.; Rubin, R. H.; Fischman, A. J. *J. Nucl. Med.* **1993**, *34*, 1964.

(6) (a) Re-188 Generators are currently available for clinical cancer treatment: Ehrhardt, G. J.; Ketring, A. R.; Liang, Q.; Wolfangel, R. G. *J. Nucl. Med.* **1993**, *34*, 38P. (b) Ehrhardt, G. J.; Ketring, A. R.; Liang, Q.; Wolfangel, R. G. *J. Nucl. Med.* **1993,** *34*, 38P.

(7) Babich, J. Unpublished data.

Despite the manifest potential of bifunctional organohydrazino ligands in protein radiolabeling for nuclear medicinal applications, the nature of the metal coordination to the HYNIC linker has not been elucidated nor has the influence of coligands been addressed systematically. Since radiolabeling is achieved by reaction of $[MO_4]^-$ (M = Tc or Re) with a reducing agent in the presence of a weakly coordinating chelating ligand, it has been assumed that metal incorporation occurs through a condensation reaction, resulting in the formation of the robust metal−hydrazido coordination unit, {M = NNR},[8] which is characteristic of oxorhenium chemistry with organohydrazines.[9] However, the absence of model compounds of Tc or Re with hydrazinopyridine derivatives rendered such arguments speculative at best and suggested that the coordination chemistry of Tc and Re with hydrazinopyridine should provide some insights into the nature of the chemistry on the tracer scale. Furthermore, the demonstration that coligands, such as sugars and thiolates, radically influence the biodistribution of the ^{99m}Tc-labeled HYNIC-derivatized chemotactic peptides provided further impetus for development of the Tc− and Re−hydrazinopyridine coordination chemistry.[5b]

In this paper, we present the details of the preparation of the {^{99m}Tc−(pyrimidine-2-thiol)−HYNIC−peptide} imaging agent and its imaging properties. In order to define some structural possibilities for the coordination chemistry relevent to these reagents, we also present the results of our investigations of the syntheses and structures of Tc, Mo, and Re complexes with hydrazinopyridine, which not only establish the formation of the robust {M = NNR} unit, but also implicate chelate formation through the pyridine nitrogen as a significant structural determinant. The structures of the parent (bis)hydrazino−trichlorometalate core compounds **2**−**6** are presented, allowing analysis of structural changes that occur when (i) protonation sites on the ligand change, (ii) a different metal is employed, and (iii) a different chelating hydrazine is utilized. The structures of the thiolate substitution products of these parent compounds are also presented. These derivatives demonstrate that rhenium and technetium have analogous substitution chemistry, resulting in the formation of $[Re(C_5H_4NS)_2(NNC_5H_4N)(HNNC_5H_4N)]$ (**8**), $[Re(C_4H_3N_2S)_2(NNC_5H_4N)(HNNC_5H_4N)]$ (**9**), $[Re(C_9H_6NS)_2(NNC_5H_4N)(HNNC_5H_4N)]$ (**10**), and $[Tc(C_5H_4NS)_2(NNC_5H_4N)(HNNC_5H_4N)]$ (**7**). Analogously, reaction of the molybdate parent complex $[MoCl_3(NNC_5H_4NH)(HNNHC_5H_4N)]$ (**6**) with pyrimidine-2-thiol yields $[Mo(C_4H_3N_2S)_2(NNC_5H_4N)(HNNHC_5H_4N)]$ (**11**) and $[Mo(C_4H_3N_2S)_3(NNC_5H_4N)]$ (**12**).

Experimental Section

General Methods. All solvents were of reagent grade and were used as received. Ammonium perrhenate, sodium molybdate, 2-hydrazinopyridine, 2-hydrazinopyridine·2HCl, 2-hydrazino-2-imidazoline·HBr, pyrimidine-2-thiol, pyridine-2-thiol, D-mannitol, catechol, PPh_3, and NEt_3 were purchased from Aldrich. ITLC silica gel (ITLC-sg) chromatographic strips were obtained from Gelamn Laboratories (Ann Arbor, MI). ^{111}In oxime was obtained from Amersham Inc. (Arlington Heights, IL). Stannous glucoheptonate kits (Glucoscan) and ^{99}Mo/^{99m}Tc generators were obtained from DuPont radiopharmaceutical division (Bilerica, MA). All other reagents used in radiopharmaceutical preparations were obtained as the highest available grade from commercial sources. **CAUTION:** ^{99}Tc is a weak β emitter (293 keV). All experiments involving ^{99}Tc were performed in a laboratory designed for and devoted exclusively to the preparation of radioactive materials. Due to the strong possibility of contamination, and current licensing regulations for our laboratory, ^{99}Tc-containing species were characterized only by X-ray crystallography. All compounds of this study are diamagnetic as judged by NMR studies.

Peptide Synthesis. N-for-methionyl-leucyl-phenylalanyl-lysine (f-MLFK) was synthesized and purified by standard solid-phase techniques[10,11] as previously described. The nicotinylhydrazine conjugate of this peptide, N-for-Met-Leu-Phe-(N-ϵ-HYNIC)-Lys (HP), was prepared as previously described.[5c] The product was purified by reverse phase HPLC on a 2.5 × 50 cm Whatman ODS-3 column eluted with a gradient of water/acetonitrile in 0.1% TFA. Fractions containing the major component were combined and the solvent was removed to yield the desired product. The peptide was charcterized by UV and mass spectroscopy as well as amino acid analysis.

Preparation of ^{99m}Tc−Mannitol. A solution of Sn(II) mannitol was prepared by dissolving 800 mg of mannitol (Aldrich) in dilute HCl followed by the dropwise addition of 1 mg of stannous chloride in 1 N HCl. All solutions were purged with nitrogen prior to and during manipulation. The pH of the final Sn(II) mannitol solution was adjusted to between 5 and 6 with NaOH. The final concentrations of "coligand" and Sn(II) (as $Sn^{II}Cl_2$) were ∼80 mg/mL and 100 μg/mL, respectively. The solution was filtered using a 0.22 μm Miller GS filter, and 0.5 mL aliquots were transferred to sterile rubber stoppered glass vials, purged with N_2, and stored at −70 °C until use.

^{99m}Tc−mannitol was prepared by adding 2.0 mL of $^{99m}TcO_4^-$ in saline to a 0.5 mL aliquot of Sn(II) mannitol solution. The solution was vortexed briefly and let stand at room temperature for 5 min before determination of radiochemical purity (RCP). The final concentration of radioactivity was 5−10 mCi/mL. Radiochemical analysis was performed using ITLC-sg with two solvents: acetone and saline. The R_f's of ^{99m}Tc−mannitol were 0.0 and 1.0 in acetone and saline, respectively. Potential impurities are TcO_4^- and TcO_2.

^{99m}Tc Labeling of HYNIC-Derivatized Chemotatic Peptides. The following procedure was used to radiolabel the chemotactic peptide analogue with ^{99m}Tc. Five microliters of a 1 mg/mL peptide solution was transferred to a clean glass vial whereupon 500 μL of 0.1 M acetate buffer pH 5.2 was added to this peptide solution followed by 500 μL ^{99m}Tc−mannitol. The mixture was vortexed briefly and allowed to stand at room temperature for 1 h. Radiochemical purity was determined by HPLC using a C_{18} reverse phase column (300 Å, 5μ, 4.5 × 25 cm, Vydac) and the following elution conditions: solvent A, 0.1% trifluoroacetic acid in water; solvent B, 0.1% trifluoroacetic acid in acetonitrile; gradient, 0% B to 100% B over 10 min; flow rate, 2 mL/min. UV absorption was monitored with a flow-through spectrometer (Milton-Roy/LDC, Boca Raton, FL), and radioactivity was monitored using a radioisotope detector (Beckman 170, Beckman, Columbia, MD). The outputs from both detectors were recorded and analyzed using a dual-channel integrator (Waters model 746 data module, Waters, Marlboro, MA).

Conversion to the thiolate-containing complex was accomplished by incubation of equal volumes of pyrimidinethiol or pyridinethiol (1 mg/mL DMSO) and Tc−peptide at room temperature for 1 h. The labeled complex was characterized by C_{18} reverse phase HPLC. Injectable solutions of {^{99m}Tc(PT)−HP} were prepared by isolating the {^{99m}Tc(PT)−HP} from the unlabeled HP using the HPLC system described above. The peptide solution was gently heated and dried under a stream of N_2. The residue was dissolved in isotonic saline for injection. A sample of the injectate was analyzed by HPLC. The isolated peaks were run only once prior to injection in animals and were found to be stable over a period of approximately 2 h. No

(8) (a) Abrams, M. J.; Larsen, S. K.; Zubieta, J. *Inorg. Chim. Acta* **1990**, *171*, 133. (b) Abrams, M. J.; Chen, Q.; Shaikh, S. N.; Zubieta, J. *Inorg. Chim. Acta* **1990**, *176*, 11. (c) Nicholson, T.; Davison, A.; Jones, A. G. *Inorg. Chim. Acta* **1990**, *168*, 227. (d) Archer, C. M.; Dilworth, J. R.; Jobanputra, P.; Thompson, R. M.; McPartlin, M.; Povey, D. C.; Smith, G. W.; Kelly, J. D. *Polyhedron* **1990**, *9*, 1497.

(9) (a) Nicholson, T.; Zubieta, J. *Polyhedron* **1988**, *7*, 171. (b) Chatt, J.; Dilworth, J. R.; Leigh, G. J.; Gupta, V. D. *J. Chem. Soc. A* **1971**, 2631. (c) Nicholson, T.; Shaikh, N.; Zubieta, J. *Inorg. Chim. Acta* **1985**, *99*, L45. (d) Dilworth, J. R.; Harrison, S. A.; Walton, D. R. M.; Schweda, E. *Inorg. Chem.* **1985**, 24, 2594. (e) Sutton, D. *Chem. Soc. Rev.* **1975**, 443.

(10) Merrifield, R. B. *J. Am. Chem. Soc.* **1963**, *85*, 2149.

(11) Stewart, J. M.; Young, J. D. *Solid-Phase Peptide Synthesis*; Freeman: San Francisco, CA, 1969.

Table 1. Infected to Normal Muscle Ratios for ^{99m}Tc−f-MLFK−HYNIC Labeled via Mannitol or Pyridine-2-thiol in Rabbits with *E. coli* Infection

	infected:normal muscle ratios[b,c]	
coligand[a]	3 h	18 h
pyridinethiol	4.042 ± 0.548	9.601 ± 0.837
mannitol	3.906 ± 0.316	11.886 ± 2.205

[a] There is no significant difference between peptide preparations. [b] Times after injection. [c] The animals were infected 24 h before radiopharmaceutical injection. Each value is the mean ± sem for 6 animals.

Table 2. Biodistribution of ^{99m}Tc−Peptides[c]

organ	mannitol	pyridinethiol
blood	0.019 ± 0.0026	0.019 ± 0.0024
heart	0.033 ± 0.0029	0.025 ± 0.002
lung[b]	0.324 ± 0.0411	0.100 ± 0.0257
liver[b]	0.382 ± 0.0364	0.231 ± 0.0116
spleen	0.944 ± 0.1477	0.579 ± 0.0225
kidney	0.157 ± 0.0147	0.128 ± 0.1277
adrenal	0.059 ± 0.0059	0.058 ± 0.0106
stomach	0.032 ± 0.0031	0.045 ± 0.0088
GI tract[a]	0.029 ± 0.0024	0.095 ± 0.004
testes[b]	0.013 ± 0.001	0.007 ± 0.0011
muscle	0.002 ± 0.0002	0.002 ± 0.0002
marrow	0.172 ± 0.0184	0.151 ± 0.0055
bone	0.024 ± 0.005	0.016 ± 0.0015

[a] Significant difference between peptide preparations at $p < 0.01$. [b] Significant difference between peptide preparations at $p < 0.05$. [c] Values are mean ± sem; values are for 6 animals.

Table 3. Concentrations of ^{99m}Tc−Peptides in Normal Muscle, Infected Muscle, and Pus Determined by Direct Measurements of Radioactivity[b]

coligand[a]	infected muscle	pus	normal muscle
mannitol	0.100 ± 0.0076	0.247 ± 0.049	0.0021 ± 0.0002
pyridinethiol	0.095 ± 0.0152	0.311 ± 0.102	0.0017 ± 0.0002

[a] There is no significant difference between peptide preparations. [b] Mean ± sem, $n = 6$.

subsequent stability studies per se were performed. Specific activity was >10 000 Ci/mmol postpurification and was calculated using the relation (% RCP × mCi present)/(μmol of peptide × 100).

Infection Model and Imaging. Male New Zealand white rabbits weighing 2.5−3.0 kg were used in all studies. *Escherichia coli* samples were obtained from a single clinical isolate, grown overnight on trypticase soy agar plates, and individual colonies were diluted with sterile saline to produce a suspension containing about 1×10^{11} organisms/mL. A 0.5 mL inoculum of the bacterial suspension was injected deep in the left thigh muscle of the rabbits. Twenty-four hours after inoculation, rabbits with gross swelling in the infected thigh were injected with 1 mCi of HPLC-purified {^{99m}Tc−(pyrimidine-2-thiol)−HP} (specific activity > 10 000 mCi/μmol) through a lateral ear vein. The animals were anesthetized with ketamine and xylazine (15.0 and 1.5 mg/kg), and scintigrams were acquired at 3 and 18 h postinjection using a LFOV γ camera using a high-resolution parallel hole collimator (Technicare 560, Solon, OH). Images were recorded for a preset time of 5 min/view with a 15% window centered to include the 140 keV photopeak of ^{99m}Tc. To characterize the localization of labeled peptide, a region-of-interest (ROI) analysis was performed, comparing the infected thigh to the contralateral normal thigh muscle as a function of time, as shown in Table 1. After the final images were acquired, the animals were sacrificed by pentobarbital overdose, tissue samples were excised and weighed, and radioactivity was measured using a scintillation counter, the results of which are shown in Table 2. Comparasion uptake levels of infected muscle, normal muscle, and pus are presented in Tables 3 and 4.

The results of the imaging studies were evaluated by two-way analysis of variance (ANOVA) with a linear model in which peptide and time were the classification variables: target/background = coligand + time + (coligand × time). The results of the bidistribution studies were evaluated by two-way ANOVA with a linear model in which organ and mannitol were the classification variables: % ID/g or % ID/organ = organ + coligand + (organ × coligand). Post hoc comparisons of peptide concentrations were performed by Duncan's new multiple range test.[12] All results are expressed as the mean ± sem, where sem is the standard error of the mean.

Table 4. Target to Background Ratios of ^{99m}Tc−Peptides for Infected Muscle and Pus Determined by Direct Measurements of Radioactivity[b]

coligand[a]	infected muscle:normal muscle	pus:normal muscle
mannitol	49.84 ± 3.60	99.19 ± 23.28
pyridinethiol	56.71 ± 8.85	202.27 ± 90.51

[a] There is no significant difference between peptide preparations. [b] Mean ± sem, $n = 6$.

Preparation of [$TcCl_3(\eta^1$-$NNC_5H_4NH)(\eta^2$-$HNNC_5H_4N)$] (2). A stock solution of $[NH_4][TcO_4]$ (0.0459 mmol) was placed in a 25 mL Schlenk flask. The solution was dried under dynamic vacuum to produce solid $[NH_4][TcO_4]$. To the white solid was added 2-hydrazinopyridine·2HCl (0.0334 g, 0.184 mmol) in 2 mL of MeOH. The reaction was stirred for 1.5 h. The black product (0.015 g, 78% yield) was collected by filtration and dried under dynamic vacuum.

Preparation of [$ReCl_3(\eta^1$-$NNC_5H_4NH)(\eta^2$-$HNNC_5H_4N)$] (3). Method 1. In a 100 mL Schlenk flask were placed [Na][ReO_4] (0.20 g, 0.74 mmol), 2-hydrazinopyridine·2HCl (0.66 g, 3.65 mmol), and 10 mL of MeOH. The reaction mixture was stirred and heated to reflux for 2 h. The mixture was cooled to room temperature, and product was collected by filtration.

Method 2. A mixture of $[NH_4][ReO_4]$ (0.5 g, 1.86 mmol), 2-hydrazinopyridine (0.81 g, 7.45 mmol), and 25 mL of MeOH was placed in a 100 mL Schlenk flask. The reaction mixture was stirred briefly, and 1.20 mL of aqueous 36% HCl (10 mmol) was added dropwise. The reaction mixture was heated to reflux for 0.3 h. The mixture was cooled to room temperature, and the product was collected by filtration. The product was washed with four 5 mL portions of MeOH and dried to give 0.860 g of **3** in a 90% yield.

Method 3. In a 100 mL Schlenk flask were placed $[NH_4][ReO_4]$ (2.0 g, 7.46 mmol), 2-hydrazinopyridine·2HCl (5.43 g, 29.8 mmol), and 50 mL of MeOH. The reaction mixture was stirred and heated to reflux for 0.5 h. The mixture was cooled to room temperature, and the product was collected by filtration, washed with two 10 mL portions of MeOH, and dried to give 3.48 g of **3** (92% yield). IR (KBr, cm^{-1}): 3090 (w), 1604 (m), 1522 (s), 1465 (w), 1442 (m), 1373 (w), 1298 (s), 1266 (m), 1232 (s), 1163 (m), 1112 (w), 891 (w), 763 (m). ^{1}H NMR (DMSO-d_6, ppm) 4.22 (s, 2H), 6.88 (dd, 1H), 7.22 (dd, 1H), 7.72 (d, 1H), 7.99 (m, 2H), 8.32 (dd, 1H), 8.32 (dd, 1H), 8.43 (d, 1H), 8.79 (d, 1H). Crystals were grown by diffusion of MeOH into a DMF solution of **3**. Anal. Calcd for $C_{10}H_{10}Cl_3N_6Re$: C, 23.7; H, 1.97; N, 16.6. Found: C, 23.8; H, 2.01; N, 15.8.

Preparation of [$HNEt_3$][$ReCl_3(\eta^1$-$NNC_5H_5N)(\eta^2$-$HNNC_5H_4N)$]·H_2O (4). A mixture of **3** (0.100 g, 0.197 mmol), NEt_3 (0.059 g, 0.591 mmol), and 10 mL of ethanol was placed in a 50 mL Schlenk flask. The reaction mixture was stirred for 60 h, and then the solution was dried under vacuum. The dark green crystals of **4** were grown by slow diffusion of pentane into a CH_2Cl_2 solution of **4** (yield: 0.048 g, 41%). IR (KBr, cm^{-1}): 3448 (s), 2974 (w), 2940 (w), 2678 (m), 2628 (m), 2493 (w), 1618 (m), 1578 (m), 1560 (m), 1534 (m), 1508 (w), 1474 (m), 1458 (m), 1420 (s), 1340 (m), 1309 (m), 1243 (m), 1209 (m), 1144 (w), 1071 (w), 1032 (w), 779 (m), 692 (w). ^{1}H NMR (DMSO-d_6, ppm): 6.80 (dd, 1H), 6.95 (dd, 1H), 7.15 (d, 1H), 7.66 (d, 1H), 7.85 (m, 2H), 8.15 (s, 1H), 8.57 (d, 1H), 8.82 (d, 1H).

Preparation of [$ReCl_3(\eta^1$-$NNC_3H_4N_2H)(\eta^2$-$HNNHC_3H_4N_2H)$] (5). The reactants NH_4ReO_4 (0.200 g, 0.745 mmol), 2-hydrazine-2-imidazoline·HBr (0.538 g, 2.98 mmol), and 36% HCl (0.110 g, 2.98 mmol) were placed in 10 mL of MeOH in a 50 mL Schlenk flask. The reaction mixture was stirred and refluxed overnight. The mixture was cooled to room temperature, and the product was collected by filtration.

(12) Duncan, D. B. *Biometrics* **1955**, *11*, 1−42.

The product was air-dried to give **5** in 67% yield (0.241 g). IR (KBr, cm^{-1}): 3288 (m), 1563 (s), 1522 (s), 1497 (s), 1341 (m), 1280 (m), 1223 (s), 1089 (m), 918 (w), 855 (w). Dark red crystals of **5** were grown by slow diffusion of pentane into a CH_2Cl_2 solution of **5**.

Preparation of [$MoCl_3(\eta^1$-$NNC_5H_4NH)\{\eta^2$-$HNNH(C_5H_4N)\}$] (6). Method 1. A mixture of Na_2MoO_4 (0.050 g, 0.198 mmol), hydrazidopyridine (0.144 g, 0.132 mmol), and 36% HCl (0.029 g, 0.794 mmol) in 6 mL of CH_3CN was placed in a glass tube. The contents were frozen in liquid nitrogen, and the tube was flame sealed under vacuum to give a 32% fill volume. The tube was placed in an oven at 110 °C for 3 days. Dark red crystals were produced in a 45% yield.

Method 2. A mixture of Na_2MoO_4 (0.200 g, 0.823 mmol) and hydrazinopyridine·2HCl (0.598 g, 3.30 mmol) in 20 mL of MeOH was placed in a 100 mL Schlenk flask. The reaction mixture was stirred and refluxed overnight. The mixture was cooled to room temperature, and the product was collected by filtration. The brick red product was allowed to air-dry to give 0.324 g of **6** in 94% yield. IR (KBr, cm^{-1}): 3022 (m), 1618 (s), 1597 (s), 1560 (w), 1513 (m), 1446 (m), 1424 (s), 1370 (m), 1314 (m), 1277 (s), 1184 (m), 1156 (m), 998 (m), 872 (w), 753 (s), 616 (w), 495 (w). Anal. Calcd for $C_{10}H_{11}N_6Cl_3Mo$: C, 28.8; H, 2.64; N, 20.1. Found: C, 28.5; H, 2.67; N, 19.8.

Preparation of [$Tc(C_5H_4NS)_2(\eta^1$-$NNC_5H_4N)(\eta^2$-$HNNC_5H_4N)$] (7). Compound **2** was suspended in 3 mL of MeOH, and pyridine-2-thiol (0.009 g, 0.0814 mmol) in 1.5 mL of MeOH was added. The mixture was stirred briefly, and NEt_3 (0.017 mL, 0.122 mmol) was added. The resultant dark red solution was stirred for 1 h, whereupon the reaction mixture was dried under vacuum to yield a mixture of **7** and $HNEt_3Cl$. Crystals were grown by diffusion of pentane into a solution of **7** in CH_2Cl_2.

Preparation of [$Re(C_5H_4NS)_2(\eta^1$-$NNC_5H_4N)(\eta^2$-$HNNC_5H_4N)$] (8). Compound **3** (0.200 g, 0.396 mmol) and pyridine-2-thiol (0.087 g, 0.784 mmol) were mixed with 20 mL of ethanol and NEt_3 (0.120 g, 1.19 mmol) in a 50 mL Schlenk flask. The reaction mixture was stirred and refluxed overnight. This reaction mixture was evaporated to dryness and suspended in 50 mL of H_2O. This black material was subsequently collected by filtration and washed with two 25 mL portions of H_2O and Et_2O. The product was oven-dried to yield 0.254 g of **8** in 95% yield. IR (KBr, cm^{-1}): 3066 (vw), 3028 (w), 1629 (s), 1578 (vs), 1553 (s), 1458 (m), 1440 (m), 1421 (vs), 1244 (m), 1212 (m), 1146 (m), 1116 (m), 760 (s). ^1H NMR (CD_2Cl_2): multiple peaks between 6.48 and 9.10 ppm. Anal. Calcd for $C_{20}H_{17}N_8S_2Re$: C, 38.8; H, 2.75; N, 18.1. Found: C, 38.4; H, 2.52; N, 17.8.

Preparation of [$Re(C_4H_3N_2S)_2(\eta^1$-$NNC_5H_4N)(\eta^2$-$HNNC_5H_4N)$] (9). Compound **3** (0.050 g, 0.098 mmol), pyrimidine-2-thiol (0.022 g, 0.20 mmol), and 10 mL of ethanol and NEt_3 (0.029 g, 0.29 mmol) were mixed in a 100 mL Schlenk flask. The reaction mixture was stirred and refluxed overnight to produce **9** as a black solid, which was collected by filtration and allowed to dry in air (0.042 g, 68% yield). IR (KBr, cm^{-1}): 3450 (m), 1686 (w), 1622 (s), 1606 (s), 1550 (s), 1458 (m), 1421 (vs), 1372 (vs), 1294 (s), 1242 (m), 1225 (m), 1167 (m), 1148 (m), 1014 (w), 822 (w), 763 (m), 752 (m), 741 (w), 600 (w). ^1H NMR (DMSO-d_6, ppm): 6.84 (dd), 6.93 (dd), 7.23 (d), 7.40 (s), 7.64 (d), 7.67 (dd), 7.70 (d), 7.83 (d), 7.87 (d), 7.97 (d), 8.23 (s), 8.36 (d) and 8.76 (s). Anal. Calcd for $C_{18}H_{15}N_{10}S_2Re$: C, 34.8; H, 2.41; N, 22.5. Found: C, 34.8; H, 2.18; N, 22.6. Crystals of **9** were grown by diffusion of pentane into a solution of **9** in CH_2Cl_2.

Preparation of [$Re(C_9H_6NS)_2(\eta^1$-$NNC_5H_4N)(\eta^2$-$HNNC_5H_4N)$] (10). A mixture of **3** (0.050 g, 0.098 mmol), quinoline-2-thiol (0.095 g, 0.59 mmol) in 15 mL of ethanol, and NEt_3 (0.059 g, 0.59 mmol) was placed in a 100 mL Schlenk flask. The reaction mixture was stirred overnight to produce an olive green solid **10**, which was collected by filtration and allowed to dry in air (0.117 g, 82% yield). IR (KBr, cm^{-1}): 3450 (w), 1616 (m), 1549 (s), 1498 (w), 1458 (m), 1420 (vs), 1299 (s), 1239 (m), 1208 (m), 1144 (w), 1112 (w), 1081 (m), 818 (w), 771 (m), 600 (w). Anal. Calcd for $C_{28}H_{21}N_8S_2Re$: C, 46.7; H, 2.91; N, 15.6. Found: C, 47.0; H, 2.95; N, 15.5. Crystals were grown by slow diffusion of pentane into a CH_2Cl_2 solution of **10**, but the poor crystal quality did not allow a satisfactory structural analysis.

Preparation of [$Mo(C_4H_3N_2S)_2(\eta^1$-$NNC_5H_4N)(\eta^2$-$HNNHC_5H_4N)$] (11). Compound **6** (0.100 g, 239 mmol), pyrimidine-2-thiol (0.161 g, 144 mmol), 15 mL of methanol, and NEt_3 (0.145 g, 144 mmol) were mixed in a 50 mL Schlenk flask. The reaction mixture was stirred and refluxed overnight. The solution was filtered, and the green precipitate was air-dried (0.130 g, 95% yield). IR (KBr, cm^{-1}): 3055 (w), 1608 (s), 1560 (w), 1540 (m), 1508 (s), 1448 (m), 1414 (s), 1374 (s), 1330 (m), 1246 (w), 1226 (s), 1186 (s), 1143 (m), 1053 (w), 984 (m), 794 (m), 762 (m), 751 (m), 738 (m), 636 (w), 485 (w), 471 (w). Anal. Calcd for $C_{18}H_{16}N_{10}S_2Mo$: C, 40.5; H, 2.99; N, 26.2. Found: C, 41.2; H, 3.41; N, 25.4.

Preparation of [$Mo(C_4H_3N_2S)_3(\eta^1$-$NNC_5H_4N)]\cdot CH_2Cl_2$ (12). Compound **6** (0.100 g, 239 mmol) was mixed with pyrimidine-2-thiol (0.161 g, 144 mmol) in 15 mL of methanol and NEt_3 (0.145 g, 144 mmol) in a 50 mL Schlenk flask. The reaction mixture was stirred and refluxed overnight, whereupon the solution was filtered and the red filtrate was dried under vacuum. Red crystals of **12** were grown by slow diffusion of pentane into a CH_2Cl_2 solution of **12**. The typical yield is 10−20 crystals (ca. 0.010 g). Due to the small amount of product, further characterization was not possible.

Preparation of [$Re(C_8H_6O_4)(PPh_3)(\eta^1$-$NNC_5H_4N)(\eta^2$-$HNNC_5H_4N)$] (13). Compound **3** (1.17 g, 2.32 mmol) was mixed with 3,4-dihydroxymethylbenzoate (0.390 g, 2.32 mmol) and triphenylphosphine (0.607 g, 2.32 mmol) in 75 mL of ethanol and NEt_3 (0.950 g, 9.40 mmol) in a 100 mL Schlenk flask. The reaction mixture was stirred and refluxed overnight to produce a black solution. The reaction mixture was evaporated to dryness and then washed with 50 mL of H_2O and 100 mL of EtOH. IR (KBr, cm^{-1}): 3058 (m), 2943 (w), 1701 (s), 1560 (s), 1542 (m), 1488 (s), 1460 (m), 1421 (vs), 1278 (s), 1241 (m), 1082 (m), 768 (m), 694 (w), 524 (m). The black product (0.622 g, 32% yield) was collected by filtration and allowed to dry in air. Anal. Calcd for $C_{36}H_{30}N_6O_4PRe$: C, 52.2; H, 3.62; N, 10.2. Found: C, 52.6; H, 3.71; N, 10.4. ^{31}P NMR (EtOH, ppm): 21.48 (s).

Preparation of [$Re(C_6H_{12}O_6)(\eta^1$-$NNC_5H_4N)(\eta^2$-$HNNC_5H_4N)$] (14). Compound **3** (0.20 g, 0.393 mmol) was mixed with D-mannitol (0.143 g, 0.786 mmol) in 25 mL of ethanol and NEt_3 (0.200 g, 1.98 mmol) in a 100 mL Schlenk flask. The reaction mixutre was stirred and refluxed overnight to produce a black solution. The reaction mixture was evaporated to dryness and then washed with 15 mL of Et_2O, 15 mL of CH_2Cl_2, and 15 mL of H_2O. The black product (164 mg, 72% yield) was collected by filtration and allowed to dry in air. IR (KBr, cm^{-1}): 3322 (m), 2931 (w), 1607 (s), 1534 (s), 1459 (m), 1459 (s), 1420 (vs), 1295 (s), 1212 (m), 1148 (m), 1015 (w), 771 (m), 669 (w). Anal. Calcd for $C_{16}H_{21}N_6O_6Re$: C, 33.1; H, 3.62; N, 14.5. Found: C, 32.8; H, 3.89; N, 12.6. The discrepancy in the nitrogen analysis reflects the formation of nonvolatile rhenium−nitrido species. It is not unusual for nitrogen analysis of metal−hydrazido complexes to be one nitrogen short.

X-ray Crystallography. All compounds were studied with graphite-monochromated Mo Kα radiation (λ(Mo Kα) = 0.710 73 Å). Compounds **5** and **7**−**9** were studied using a Rigaku AFC5S diffractometer, equipped with a low-temperature device. The small size of crystals of **3** necessitated the use of a Rigaku AFC7R diffractometer. The crystals of **4**, **6**, and **12** were studied using a Siemens SMART diffractometer. Since the crystals of **5** and **7**−**9** degraded slowly at room temperature, data collections were carried out at low temperature. Crystal stability was monitored using three medium-intensity reflections after every 150 reflections, and in each case no significant changes in the intensities of the standards were observed over the course of the data collections. The crystal parameters and other experimental details of the data collections are summarized in Table 5. For compounds **3**, **4**, **7**, **8**, and **12,** data collection was carried out to a 2θ of 45° only as the reflection intensities decreased precipitously above 40° in 2θ, yielding 10−20% observables. An empirical absorption correction using the program DIFABS was applied to the data for **4**,[13] while all other data sets employed absorption corrections based on ψ scans. The data were corrected for Lorentz and polarization effects. The structures were solved by direct methods.[14] Metal and coordinated atoms were refined anisotropically. Neutral atom scattering factors were taken from Cromer and Waber,[15] and anomalous dispersion corrections were taken from

(13) Walker, N.; Stuart, D. *Acta Crystallogr., Sect. A* **1983**, *39*, 158.
(14) *teXsan: Texray Structural Analysis Package*, revised; Molecular Structure Corporation: The Woodlands, TX, 1992.
(15) Cromer, D. T.; Waber, J. T. *International Tables for X-ray Crystallography*; Kynoch Press: Birmingham, England, 1974; Vol. IV.

Table 5. Crystallographic Data for $[ReCl_3(NNC_5H_4NH)(HNNC_5H_4N)]$ (**3**), $[HNEt_3][ReCl_3(NNC_5H_4N)(HNNC_5H_4N)]$ (**4**), $[ReCl_3(NNC_3H_4N_2H)(HNNHC_3H_4N_2H)]$ (**5**), $[MoCl_3(NNC_5H_4NH)(HNNHC_5H_4N)]$ (**6**), $[Tc(C_5H_4NS)_2(NNC_5H_4N)(HNNC_5H_4N)]$ (**7**), $[Re(C_5H_4NS)_2(NNC_5H_4N)(HNNC_5H_4N)]$ (**8**), $[Re(C_4H_3N_2S)_2(NNC_5H_4N)(HNNC_5H_4N)]$ (**9**), and $[Mo(C_4H_3N_2S)_3(HNNC_5H_4N)]$ (**12**)

	3	**4**	**5**	**6**	**7**	**8**	**9**	**12**
empirical formula	$C_{10}H_{10}Cl_3N_6Re$	$C_{16}H_{27}Cl_3N_7ORe$	$C_6H_{12}Cl_3N_8Re$	$C_{10}H_{11}Cl_3N_8Mo$	$C_{20}H_{17}N_8S_2Tc$	$C_{20}H_{17}N_8S_2Re$	$C_{18}H_{15}N_{10}S_2Re$	$C_{18}H_{15}Cl_2N_9S_3Mo$
a, Å	7.527(2)	7.5031(1)	9.093(2)	15.386(3)	8.827(2)	8.848(2)	8.796(2)	10.5290(1)
b, Å	7.599(2)	10.3643(2)	11.105(2)	7.804(2)	9.278(2)	9.190(2)	9.008(2)	15.1116(3)
c, Å	13.118(3)	30.1590(5)	14.295(3)	12.387(3)	13.304(3)	13.293(3)	13.208(3)	15.8193(3)
α, deg	106.55(3)							
β, deg	90.28(3)		94.71(3)	95.92(3)	98.92(3)	98.89(3)	97.90(3)	108.479(1)
γ, deg	93.83(3)							
V, Å^3	717.4(4)	2345.20(6)	1438.6(7)	1476.4(5)	1076.5(5)	1067.9(5)	1036.6(5)	2387.23(7)
Z	2	2	4	4	2	2	2	4
fw	506.8	633.96	488.79	417.54	531.5	619.7	621.72	620.39
space group	$P\bar{1}$	$P2_12_12_1$	$P2_1/n$	$P2_1/c$	$P2_1$	$P2_1$	$P2_1$	$P2_1/n$
T, °C	25	25	−20	25	−20	−20	25	−20
λ, Å	0.710 73	0.710 73	0.710 73	0.710 73	0.710 73	0.710 73	0.710 73	0.710 73
D_{calc}, g cm^{-1}	5.544	1.773	2.257	1.907	1.640	1.927	1.992	1.721
μ, mm^{-1}	9.025	2.767	8.999	1.429	0.888	5.911	6.092	1.063
R^a	0.0360	0.0311	0.0525	0.0434	0.0605	0.0238	0.0623	0.0387
$R_w{}^b$	0.0420				0.0664	0.0308		
w$R_2{}^c$		0.0821	0.1365	0.0854			0.1045	0.1020

[a] $\sum||F_o| - |F_c||/\sum|F_o|$. [b] $[\sum w(|F_o| - |F_c|)^2/\sum w|F_o|^2]^{1/2}$. [c] $[\sum[w(F_o^2 - F_c^2)^2]/\sum[w(F_o^2)^2]]^{1/2}$.

Table 6. Atomic Positional Parameters (×10^4) and Isotropic Temperature Factors (Å^2 × 10^3) for $[ReCl_3(NNC_5H_4NH)(HNNC_5H_4N)]$ (**3**)

	x	*y*	*z*	*U*(eq)[a]
Re	2298(1)	359(1)	2795(1)	31(1)
Cl(1)	377(4)	375(4)	6415(2)	41(1)
Cl(2)	−4781(4)	−1565(4)	8035(2)	44(1)
Cl(4)	−443(4)	−1266(4)	8415(2)	46(1)
N(1)	−3684(14)	−255(13)	5979(7)	36(4)
N(2)	−3924(11)	−1541(11)	5073(7)	32(3)
N(3)	−2345(12)	−3042(10)	6051(7)	30(3)
N(4)	−2632(12)	1919(10)	7880(7)	35(3)
N(5)	−2978(14)	3576(12)	8181(7)	44(4)
N(6)	−2217(17)	3676(16)	10021(9)	58(5)
C(1)	−3146(13)	−3072(14)	5129(8)	31(4)
C(2)	−3232(16)	−4682(14)	4265(9)	40(4)
C(3)	−2531(14)	−6245(14)	4363(9)	38(4)
C(4)	−1773(15)	−6181(14)	5329(9)	40(4)
C(5)	−1703(14)	−4592(13)	6163(9)	33(4)
C(6)	−2717(15)	4434(14)	9236(8)	34(4)
C(7)	−3064(14)	6241(12)	9527(7)	27(3)
C(8)	−2079(17)	4768(19)	11064(10)	56(5)
C(9)	−2442(18)	6607(18)	11319(10)	56(5)
C(10)	−2894(18)	7299(17)	10537(11)	56(5)

[a] Equivalent isotropic *U* defined as one-third of the trace of the orthogonalized $\mathbf{U}_{ij}$ tensor.

Table 7. Atomic Positional Parameters (×10^4) and Isotropic Temperature Factors (Å^2 × 10^3) for $[HNEt_3][ReCl_3(NNC_5H_4N)(HNNC_5H_4N)]$ (**4**)

	x	*y*	*z*	*U*(eq)[a]
Re(1)	3974(1)	1276(1)	8776(1)	28(1)
Cl(1)	4846(4)	3026(3)	8289(1)	47(1)
Cl(2)	3467(4)	−377(2)	9325(1)	48(1)
Cl(3)	7101(3)	983(2)	8913(l)	42(1)
N(1)	1542(10)	1889(7)	8783(3)	35(2)
N(2)	832(11)	2786(7)	9047(3)	42(2)
N(3)	3796(13)	2681(7)	9300(3)	37(2)
N(4)	3545(9)	270(7)	8323(2)	33(2)
N(5)	3160(12)	−384(8)	7981(3)	42(2)
N(6)	225(11)	490(8)	7999(3)	39(2)
N(7)	8349(13)	−2982(8)	8763(3)	56(2)
C(1)	2118(14)	3214(9)	9340(3)	40(2)
C(2)	1730(18)	4130(10)	9662(4)	53(3)
C(3)	3030(21)	4500(12)	9956(4)	59(3)
C(4)	4709(19)	3987(11)	9918(3)	57(3)
C(5)	5052(17)	3079(10)	9596(3)	45(2)
C(6)	1433(13)	−278(9)	7802(3)	36(2)
C(7)	1066(16)	−1017(9)	7424(3)	50(2)
C(8)	−622(17)	−967(12)	7249(4)	61(3)
C(9)	−1901(17)	−186(11)	7450(4)	55(3)
C(10)	−1428(14)	526(10)	7823(3)	43(2)
C(11)	8533(37)	−2474(17)	9205(6)	47(6)
C(12)	7133(31)	−2987(17)	9506(7)	253(11)
C(13)	6857(27)	−2436(13)	8483(7)	93(6)
C(14)	6426(23)	−3178(14)	8079(5)	72(4)
C(15)	10094(25)	−2705(17)	8520(9)	141(10)
C(16)	11607(21)	−3432(18)	8694(6)	110(6)
O(1)	−2012(14)	4393(8)	8822(4)	63(3)

[a] Equivalent isotropic *U* defined as one-third of the trace of the orthogonalized $\mathbf{U}_{ij}$ tensor.

those of Creagh and McAuley.[16] All calculations were performed using SHELXTL or SHELX-93.[17]

The structures were solved by the Patterson method and refined by full-matrix least squares. Several of the compounds were refined in noncentrosymmetric space groups. The structures of the isomorphous series **7**−**9** solved and refined in the space group $P2_1$, but not in the centrosymmetric space group $P2_1/m$. The absolute configurations of **7**−**9** and **4**, which was refined in $P2_12_12_1$, were determined from their Flack *x* parameters, which were calculated for each configuration.[18,19]

The ethyl carbon atoms of the Et_3NH^+ cation of **4** exhibited large thermal motions, a feature not uncommon for alkyl ammonium groups. Carbon C12 is particularly affected, exhibiting an anomalously large thermal parameter. While the position is likely to be disordered, the electron density maps failed to reveal more than a single distinct location. Consequently, the site was modeled as a single location with a large temperature factor.

Since the locations of the hydrogen atoms are of some consequence in defining the metal−organohydrazine cores of the complexes of this study, the data for several representative structures were collected at low temperature, using either slow scan speeds with a photomultiplier tube or high-sensitivity CCD detector technology. In the instance of compounds **3**, **4**, **6**, **8**, and **12** Fourier maps revealed the locations of

(16) Creagh, D. C.; McAuley, J. W. J. *International Tables for X-ray Crystallography*; Kluwer Academic: Boston, 1992; Vol. C, Table 4.2.6.8.
(17) *SHELXTL PC*; Siemens Analytical X-ray Instruments, Inc.: Madison, WI, 1990.
(18) Flack, H. D.; Bernandinello, G. *Acta Crystallogr.* **1985**, *A41*, 500.
(19) Flack, H. D. *Acta Crystallogr.* **1983**, *A39*, 876.

Table 8. Atomic Positional Parameters ($\times 10^4$) and Isotropic Temperature Factors ($Å^2 \times 10^3$) for $[ReCl_3(NNC_3H_4N_2H)(HNNHC_3H_4N_2H)]$ (**5**)

	x	*y*	*z*	*U*(eq)[a]
Re(1)	1715(1)	726(1)	7900(1)	25(1)
Cl(1)	−385(4)	1883(3)	8389(2)	23(1)
Cl(2)	3655(4)	−693(3)	7600(2)	26(1)
Cl(3)	187(4)	−1073(4)	8077(3)	31(1)
N(1)	3167(14)	2031(13)	8137(8)	29(3)
N(2)	3902(17)	2196(12)	8924(9)	37(3)
N(3)	2487(14)	593(11)	9297(8)	25(3)
N(4)	4077(18)	1297(16)	10453(10)	46(4)
N(5)	1351(16)	1082(12)	6707(10)	33(3)
N(6)	1130(16)	1438(14)	5853(9)	41(4)
N(7)	1486(17)	984(13)	4309(9)	38(3)
N(8)	2756(16)	−92(14)	5383(9)	39(3)
C(1)	1746(19)	758(17)	5205(11)	37(4)
C(2)	2387(22)	204(20)	3737(13)	48(5)
C(3)	3105(22)	−642(16)	4497(12)	42(4)
C(4)	3500(18)	1382(15)	9548(10)	30(3)
C(5)	3298(21)	318(20)	10894(11)	45(5)
C(6)	2217(19)	−212(14)	10111(11)	39(3)

[a] Equivalent isotropic *U* defined as one-third of the trace of the orthogonalized $\mathbf{U}_{ij}$ tensor.

Table 9. Atomic Positional Parameters ($\times 10^4$) and Isotropic Temperature Factors ($Å^2 \times 10^3$) for $[MoCl_3(NNC_5H_4NH)(HNNHC_5H_4N)]$ (**6**)

	x	*y*	*z*	*U*(eq)[a]
Mo(1)	2319(1)	1289(1)	5408(1)	19(1)
Cl(1)	3636(1)	−177(1)	5868(1)	29(1)
Cl(2)	868(1)	1963(1)	4834(1)	25(1)
Cl(3)	2584(1)	−250(1)	3625(1)	25(1)
N(1)	2004(2)	2131(5)	6889(3)	25(1)
N(2)	1558(2)	1149(5)	7663(3)	28(1)
N(3)	1614(2)	−862(4)	6310(2)	21(1)
N(4)	2770(2)	3273(4)	4951(3)	24(1)
N(5)	2967(2)	4812(4)	4684(3)	28(1)
N(6)	4011(2)	6737(4)	4007(3)	24(1)
C(1)	1342(2)	−459(5)	7355(3)	22(1)
C(2)	858(3)	−1611(6)	8065(3)	28(1)
C(3)	696(3)	−3223(6)	7680(3)	30(1)
C(4)	998(3)	−3657(6)	6603(4)	29(1)
C(5)	1444(3)	−2455(5)	5950(3)	24(1)
C(6)	3807(3)	5076(5)	4227(3)	23(1)
C(7)	4819(3)	7268(6)	3610(3)	28(1)
C(8)	5472(3)	6112(6)	3366(3)	28(1)
C(9)	5296(3)	4367(6)	3565(3)	27(1)
C(10)	4468(3)	3845(6)	3985(3)	24(1)

[a] Equivalent isotropic *U* defined as one-third of the trace of the orthogonalized $\mathbf{U}_{ij}$ tensor.

all hydrogen atoms. Hydrogen atom positions and isotropic temperature factors were successfully refined to give reasonable C−H and N−H distances and unexceptional thermal parameters. The final Fourier maps revealed no excursions of electron density associated with possible hydrogen sites on hydrazine or pyridine nitrogen atoms. The assignment of hydrogen atom positions is further validated by the resultant consistent and rational description of the structures. Other details of the structure solutions and refinements are presented in the Supporting Information. No anomalies were encountered in the refinements of any of the structures. Atomic positional parameters and isotropic temperature factors for the structures are presented in Tables 6−13, and selected bond lengths and angles are given in Tables 14−21.

Results and Discussion

Imaging Properties of ^{99m}Tc-Labeled HYNIC-Derivatized Chemotactic Peptides. The nicotinylhydrazine-conjugated peptide N-for-Met-Leu-Phe-(N-ϵ-HYNIC)-Lys (HP) was treated with {^{99m}Tc−(mannitol)} solution to yield ^{99m}Tc-labeled HP. The {^{99m}Tc−(mannitol)−HP} was in turn incubated with the appropriate pyrimidinethiol or pyridinethiol (PT) to provide the {^{99m}Tc(PT)−HP} complex. For all {^{99}Tc(PT)−HP} complexes HPLC analysis showed the formation of radiochemical species with more hydrophobicity than the starting {^{99m}Tc−(mannitol)−HP}. The formation of these species was time dependent at low concentration but rapid at higher concentrations. Figure 1 shows the conversion of {Tc−mannitol−peptide} to the cor-

Table 10. Atomic Positional Parameters ($\times 10^4$) and Isotropic Temperature Factors ($Å^2 \times 10^3$) for $[Tc(C_5H_4NS)_2(NNC_5H_4N)(HNNC_5H_4N)]$ (**7**)

	x	*y*	*z*	*U*(eq)[a]
Tc(1)	2145(1)	6637	2237(1)	34(1)
S(1)	1051(3)	8603(4)	1072(2)	48(1)
S(2)	3780(3)	5593(3)	3668(2)	39(1)
N(1)	1979(11)	4983(10)	1280(7)	44(3)
N(2)	3066(11)	4643(11)	720(7)	51(3)
N(3)	4209(8)	6688(14)	1566(5)	37(2)
N(4)	404(10)	6113(9)	2631(6)	39(3)
N(5)	−786(10)	5638(11)	2892(7)	44(3)
N(6)	−899(10)	3643(10)	1796(7)	43(3)
N(7)	2585(9)	8759(10)	2852(7)	38(3)
N(8)	2966(11)	3935(11)	5087(7)	52(3)
C(1)	4295(12)	5582(12)	906(8)	40(3)
C(2)	5584(13)	5373(16)	424(8)	54(4)
C(3)	6751(13)	6336(14)	617(8)	52(5)
C(4)	6666(13)	7471(14)	1296(9)	54(4)
C(5)	5410(11)	7593(13)	1764(8)	42(3)
C(6)	−1485(11)	4357(11)	2517(8)	38(3)
C(7)	−1646(14)	2458(13)	1434(9)	55(4)
C(8)	−2932(14)	1928(16)	1760(11)	69(5)
C(9)	−3505(14)	2715(19)	2519(12)	78(6)
C(10)	−2772(12)	3930(17)	2897(10)	62(5)
C(11)	1943(11)	9640(13)	2102(7)	37(3)
C(12)	2011(13)	11124(12)	2186(10)	44(4)
C(13)	2754(11)	11739(20)	3084(9)	54(4)
C(14)	3420(12)	10813(14)	3875(9)	47(4)
C(15)	3324(11)	9338(12)	3745(8)	40(3)
C(16)	2666(12)	5214(11)	4656(8)	39(3)
C(17)	1639(12)	6189(13)	4957(8)	51(4)
C(l8)	844(14)	5780(19)	5734(10)	65(5)
C(19)	1120(17)	4436(19)	6169(10)	72(6)
C(20)	2158(16)	3597(19)	5837(9)	74(6)

[a] Equivalent isotropic *U* defined as one-third of the trace of the orthogonalized $\mathbf{U}_{ij}$ tensor.

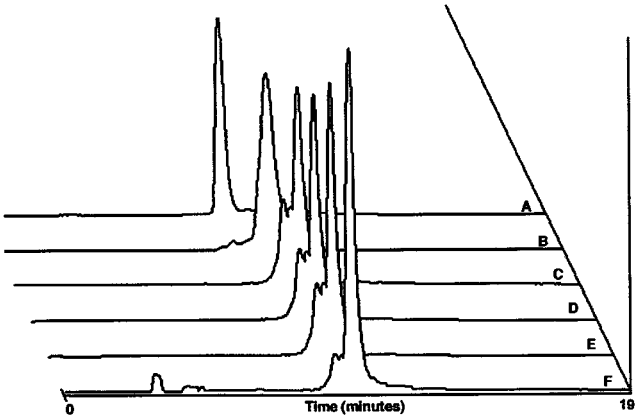

Figure 1. Effect of time on the conversion of {^{99m}Tc−(mannitol)−HYNIC−f-MLFK} (with characteristic broad peak) to the corresponding pyrimidine-2-thiol containing ^{99m}Tc−peptide complex (with a more well resolved peak): C_{18} reverse phase HPLC chromatograms showing (A) ^{99m}Tc−pyrimidine-2-thiol, (B) {^{99m}Tc−(mannitol)−HYNIC−f-MLFK}, and {^{99m}Tc−(mannitol)−HYNIC−f-MLFK} after incubation with pyridine-2-thiol after (C) 15 min, (D) 35 min, (E) 60 min, and (F) 16 h. The formation of the hydrophobic {^{99m}Tc−(pyrimidine-2-thiol)−HP} species was time dependent at low concentration but rapid at higher concentrations.

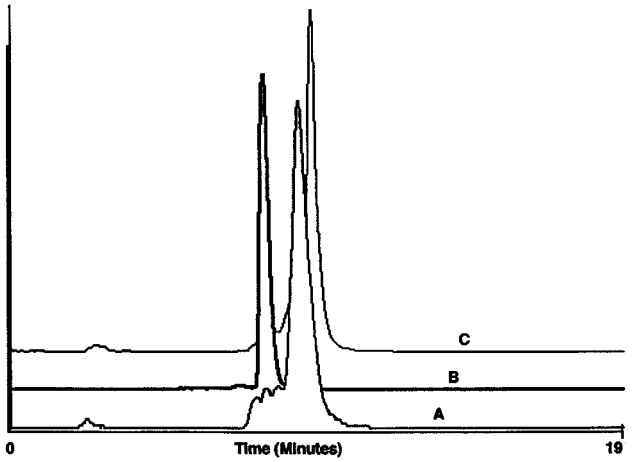

Figure 2. Illustration of the addition of the thiol ligands to the preformed Tc−mannitol−peptide complex, resulting in a Tc complex with retention times greater than those of the Tc−mannitol labeled peptide. Radio-HPLC chromatograms of (A) {^{99m}Tc−(mannitol)−HYNIC−f-MLFK}, (B) ^{99m}Tc−pyrimidine-2-thiol, and (C) {^{99m}Tc−(mannitol)−HYNIC−f-MLFK} after incubation with pyrimidine-2-thiol.

Table 11. Atomic Positional Parameters ($\times 10^4$) and Isotropic Temperature Factors (Å^2 $\times$ 10^3) for $[Re(C_5H_4NS)_2(NNC_5H_4N)(HNNC_5H_4N)]$ (**8**)

	x	*y*	*z*	*U*(eq)[a]
Re(1)	2142(1)	1220	2254(1)	24(1)
S(1)	1068(2)	−755(2)	1089(1)	36(1)
S(2)	3774(2)	2206(2)	3695(1)	29(1)
N(1)	1997(6)	2839(5)	1293(4)	30(1)
N(2)	3035(6)	3205(7)	720(4)	41(2)
N(3)	4178(4)	1191(10)	1590(3)	26(1)
N(4)	403(5)	1743(5)	2647(3)	27(1)
N(5)	−794(5)	2195(6)	2911(4)	35(2)
N(6)	−870(6)	4185(6)	1787(4)	35(2)
N(7)	2588(5)	−949(5)	2871(4)	28(1)
N(8)	2949(7)	3897(6)	5107(4)	40(2)
C(1)	4258(7)	2301(7)	914(4)	32(2)
C(2)	5549(7)	2475(8)	416(5)	40(2)
C(3)	6733(7)	1508(9)	620(5)	40(2)
C(4)	6660(7)	383(7)	1314(5)	39(2)
C(5)	5396(7)	260(7)	1781(5)	36(2)
C(6)	−1484(6)	3480(7)	2506(5)	31(2)
C(7)	−1604(8)	5402(8)	1414(5)	44(2)
C(8)	−2926(9)	5922(9)	1708(8)	61(3)
C(9)	−3532(9)	5153(10)	2466(7)	59(3)
C(10)	−2800(8)	3923(9)	2880(6)	46(2)
C(11)	1975(6)	−1806(7)	2113(4)	29(2)
C(12)	2046(7)	−3316(7)	2193(5)	38(2)
C(13)	2750(7)	−3900(13)	3094(6)	43(2)
C(14)	3408(7)	−3006(7)	3882(5)	38(2)
C(15)	3322(7)	−1535(7)	3744(4)	32(2)
C(16)	2661(7)	2583(7)	4671(4)	30(2)
C(17)	1609(7)	1611(7)	4952(5)	39(2)
C(18)	818(9)	2029(10)	5739(5)	52(3)
C(19)	1091(9)	3363(12)	6191(6)	60(3)
C(20)	2153(9)	4267(9)	5852(6)	52(3)

[a] Equivalent isotropic *U* defined as one-third of the trace of the orthogonalized $\mathbf{U}_{ij}$ tensor.

responding thiol-containing complex. Chromatogram A shows the {^{99m}Tc(PT)} complex formed by the direct reaction of {^{99m}Tc−(mannitol)} solution with pyrimidine-2-thiol.

Addition of the thiol ligands to the preformed {^{99m}Tc−(mannitol)−HP} complex resulted in Tc complexes with retention times greater than that of the Tc−mannitol labeled peptide. In the case of pyrimidine-2-thiol a primary homogeneous peak

Table 12. Atomic Positional Parameters ($\times 10^4$) and Isotropic Temperature Factors (Å^2 $\times$ 10^3) for $[Re(C_4H_3N_2S)_2(NNC_5H_4N)(HNNC_5H_4N)]$ (**9**)

	x	*y*	*z*	*U*(eq)[a]
Re(1)	2707(1)	643(1)	2695(1)	27(1)
S(1)	3773(9)	2640(9)	3880(6)	34(2)
S(2)	1085(8)	−351(8)	1242(5)	30(2)
N(1)	2849(30)	−1014(25)	3648(19)	35(6)
N(2)	1801(28)	−1360(31)	4244(16)	45(7)
N(3)	637(21)	681(45)	3354(13)	34(5)
N(4)	4420(31)	155(23)	2312(18)	42(7)
N(5)	5671(31)	−299(26)	2014(18)	42(7)
N(6)	5702(23)	−2321(26)	3157(17)	33(5)
N(7)	2175(28)	−1936(27)	−180(19)	46(6)
N(8)	3188(25)	701(60)	116(15)	43(7)
N(9)	2224(26)	2856(24)	2107(18)	39(6)
N(10)	2942(31)	5218(20)	2860(17)	37(6)
C(1)	566(29)	−386(30)	4074(20)	28(6)
C(2)	−535(31)	1700(34)	3212(22)	36(7)
C(3)	−1826(33)	1547(34)	3675(22)	42(7)
C(4)	−1858(26)	499(44)	4376(18)	37(7)
C(5)	−716(33)	−558(37)	4612(24)	48(8)
C(6)	6388(31)	−1604(31)	2489(21)	34(6)
C(7)	7740(31)	−2116(34)	2214(22)	41(7)
C(8)	8491(35)	−3299(34)	2636(22)	45(8)
C(9)	7828(31)	−4016(41)	3371(21)	53(9)
C(10)	6421(37)	−3545(37)	3568(25)	55(9)
C(11)	2285(35)	−581(36)	257(24)	44(8)
C(12)	4138(29)	271(26)	−650(20)	35(7)
C(13)	4116(34)	−945(35)	−1133(23)	44(8)
C(14)	3027(40)	−2104(43)	−923(27)	62(10)
C(15)	2978(28)	3772(29)	2875(19)	27(6)
C(16)	2313(26)	5698(95)	1966(18)	41(6)
C(17)	1679(34)	4952(33)	1074(24)	42(8)
C(18)	1642(31)	3510(31)	1174(21)	35(7)

[a] Equivalent isotropic *U* defined as one-third of the trace of the orthogonalized $\mathbf{U}_{ij}$ tensor.

was obtained (Figure 2), which when isolated and rechromatographed eluted at the same t_R.

Figure 3 shows 3 and 18 h γ images of {^{99m}Tc−(pyrimidine-2-thiol)−HP} in infected rabbits. The infected thigh muscle can clearly by delineated at 3 h, and the activity in the infected thigh is intense at 18 h. ROI analysis gave target to background values of 4.26 ± 0.97 and 9.83 ± 1.6, at 4 and 18 h, respectively. Tissue counting (18 h) resulted in a pus:normal muscle ratio of >150:1 and an infected muscle:normal muscle ratio of >50:1. At both time points gastrointestinal (GI) accumulation was evident. Whereas infection localization was similar to that with {^{99m}Tc−(mannitol)−HP}, the GI uptake would hinder the use of such a ligand system. New derivatives of PT are under development in an effort to limit GI activity while maintaining good infection localization.

Our data demonstrate that PTs can facilitate the formation of a Tc−chemotactic peptide radiochemical species with excellent infection localization. However, attempts at elucidating the structure of the thiol-containing peptide coligand complexes have not yet been successful when starting with the ^{99m}Tc−mannitol species, and it cannot be definitively demonstrated that this represents a single species. Furthermore, GI accumulation is excessive, and further work is necessary to understand the structural basis of GI accumulation in an effort to design more favorable agents.

These results further support our earlier finding that the nature of the Tc−hydrazino coordination environment has a profound effect on pharmacokinetics and excretion. Hence, appropriate formulation of low molecular weight Tc-labeled HYNIC−peptides is critical in controlling radiolabeled speciation and biological fate.

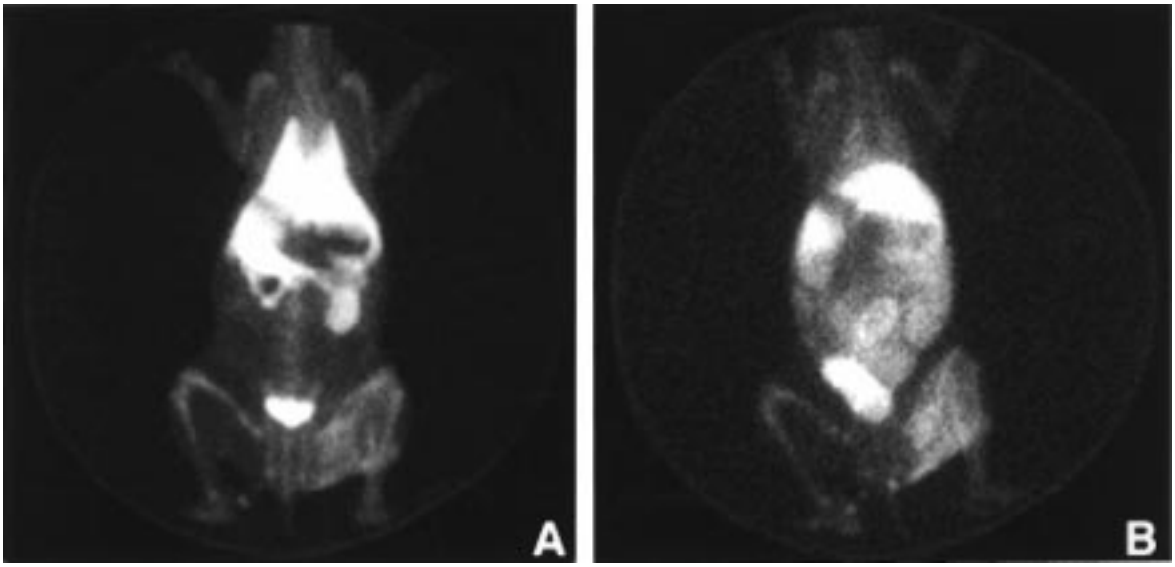

Figure 3. γ camera images of {^{99m}Tc−(pyrimidine-2-thiol)−HP} in infected rabbits at 3 h (A) and 18 h (B) postinjection. The infected thigh muscle can clearly be delineated at 3 h, and the activity in the infected thigh is intense at 18 h.

Table 13. Atomic Positional Parameters ($\times 10^4$) and Isotropic Temperature Factors (Å^2 $\times$ 10^3) for [Mo($C_4H_3N_2S$)$_3$(NNC_5H_4N)] (**12**)

	x	*y*	*z*	*U*(eq)[a]
Mo(1)	4375(1)	7488(1)	917 (1)	24(1)
S(1)	4086(1)	8575(1)	−306(1)	34(1)
S(2)	6301(1)	6898(1)	2189(1)	37(1)
S(3)	3979(1)	5844(1)	1007(1)	39(1)
Cl(1)	9151(2)	7674(1)	1096(1)	84(1)
Cl(2)	11085(1)	6249(1)	1703(1)	81(1)
N(1)	3376(3)	8013(2)	1506(2)	28(1)
N(2)	2693(3)	8439(2)	1870(2)	37(1)
N(3)	2466(4)	9569(2)	789(2)	50(1)
N(4)	5445(3)	7138(2)	−47(2)	30(1)
N(5)	5592(4)	7964(2)	−1298(2)	44(1)
N(6)	5944(3)	8449(2)	1588(2)	30(1)
N(7)	7875(3)	8328(2)	2875(2)	47(1)
N(8)	2529(3)	6965(2)	−28(2)	29(1)
N(9)	1632(4)	5513(2)	−307(3)	53(1)
C(1)	2138(4)	9270(2)	1482(2)	33(1)
C(2)	1313(5)	9711(3)	1864(3)	55(1)
C(3)	809(5)	10524(3)	1509(3)	63(1)
C(4)	1134(5)	10845(3)	792(3)	61(1)
C(5)	1946(5)	10351(3)	459(4)	65(1)
C(6)	5147(4)	7850(3)	−610(2)	32(1)
C(7)	6391(5)	7316(3)	−1423(3)	51(1)
C(8)	6722(4)	6574(3)	−902(3)	46(1)
C(9)	6226(4)	6503(3)	−204(3)	40(1)
C(10)	6820(4)	7992(3)	2258(2)	32(1)
C(11)	6120(4)	9323(3)	1553(3)	45(1)
C(12)	7199(5)	9718(3)	2171(3)	60(1)
C(13)	8046(5)	9193(3)	2804(3)	59(1)
C(14)	2545(4)	6088(3)	125(3)	36(1)
C(15)	553(5)	5868(4)	−906(3)	64(2)
C(16)	408(5)	6760(3)	−1084(3)	51(1)
C(17)	1443(4)	7311(3)	−631(3)	40(1)
C(18)	9429(5)	6597(3)	1546(3)	63(1)

[a] Equivalent isotropic *U* defined as one-third of the trace of the orthogonalized $\mathbf{U}_{ij}$ tensor.

Synthesis and Properties of Model Complexes with Metal−Hydrazido Cores. In many diagnostic and therapeutic radiopharmaceutical preparations employing ^{99m}Tc and ^{186,188}Re, these radioisotopes are eluted from the generator column as pertechnetate and perrhenate, respectively. This observation suggested the use of metal oxide starting materials in the model studies, rather than employing precursors such as $MOCl_4^-$ which are difficult to prepare under radiopharmaceutical kit conditions.

Table 14. Selected Bond Lengths (Å) and Angles (deg) for [$ReCl_3$(NNC_5H_4NH)($HNNC_5H_4N$)] (**3**)

Re(1)−Cl(1)	2.375(3)	Re(1)−Cl(2)	2.424 (3)
Re(1)−Cl(4)	2.382(3)	Re(1)−N(1)	1.936 (10)
Re(1)−N(3)	2.164(7)	Re(1)−N(4)	1.741 (7)
N(1)−N(2)	1.309(11)	N(2)−C(1)	1.357 (14)
N(3)−C(1)	1.342(14)	N(3)−C(5)	1.348 (14)
N(4)−N(5)	1.253(12)	C(1)−C(2)	1.409 (13)
C(2)−C(3)	1.369(17)	C(3)−C(4)	1.374 (17)
C(4)−C(5)	1.377(13)	N(5)−C(6)	1.359 (13)
C(6)−C(7)	1.360(13)	C(6)−N(6)	1.378 (18)
C(7)−C(10)	1.340(15)	C(8)−C(9)	1.387 (20)
C(8)−N(6)	1.382(16)	C(9)−C(10)	1.332 (21)
Cl(1)−Re(1)−Cl(2)	170.2(1)	Cl(1)−Re(1)−Cl(4)	86.3(1)
Cl(2)−Re(1)−Cl(4)	86.2(1)	Cl(1)−Re(1)−N(1)	90.9(3)
Cl(2)−Re(1)−N(1)	94.7(3)	Cl(4)−Re(1)−N(1)	164.8(3)
Cl(1)−Re(1)−N(3)	86.8(2)	Cl(2)−Re(1)−N(3)	87.2(2)
Cl(4)−Re(1)−N(3)	92.5(3)	N(1)−Re(1)−N(3)	72.5(4)
Cl(1)−Re(1)−N(4)	94.4(3)	Cl(2)−Re(1)−N(4)	93.4(3)
Cl(4)−Re(1)−N(4)	102.9(3)	N(1)−Re(1)−N(4)	92.2(4)
N(3)−Re(1)−N(4)	164.6(4)	N(2)−N(1)−Re(1)	127.1(8)
N(1)−N(2)−C(1)	109.7(9)	C(1)−N(3)−C(5)	119.5(8)
C(1)−N(3)−Re	112.2(7)	C(5)−N(3)−Re	128.2(7)
N(5)−N(4)−Re	168.1(8)	N(2)−C(1)−N(3)	118.1(8)

Furthermore, our previous investigations have shown that $ReOCl_4^-$ is too moisture sensitive for radiopharmaceutical applications.[20]

The preparations of the complexes of the general class [MCl_3(η^1-NNC_5H_4NH)(η^2-$HNNH_xC_5H_4N$)] (M = Tc (**2**), Re (**3**), x = 0; M = Mo (**6**), x = 1) are accomplished in a straightforward fashion to provide high-yield monophasic crystalline products. However, it is noteworthy that the pertechnetate and molybdate are more reactive than the perrhenate. Thus, the pertechnetate and molybdate reactions change color rapidly at room temperature while the perrhenate reaction requires 0.5 h of refluxing. Two to five equivalents of HCl is required for isolation of the desired product. Attempts to crystallize compound **2** have, to date, proved unsuccessful. It should be noted that single crystals of **3** were quite difficult to grow as well, requiring slow diffusion of alcohols into DMF solutions of the complexes over a period of several weeks.

(20) Rose, D. J.; Maresca, K. P.; Kettler, P. B.; Chang, T.-D.; Soghomomian, V.; Chen, Q.; Abrams, M. J.; Larsen, S. K.; Zubieta, J. *Inorg. Chem.* **1996**, *35*, 3548−3558.

Table 15. Selected Bond Lengths (Å) and Angles (deg) for $[HNEt_3][ReCl_3(NNC_5H_4N)(HNNC_5H_4N)]$ (**4**)

Re(1)−N(4)	1.749 (7)	Re(1)−N(1)	1.932 (8)
Re(1)−N(3)	2.151 (8)	Re(1)−Cl(3)	2.402 (2)
Re(1)−Cl(2)	2.412 (2)	Re(1)−Cl(1)	2.424 (2)
N(1)−N(2)	1.335 (11)	N(2)−C(1)	1.381 (13)
N(3)−C(5)	1.364 (13)	N(3)−C(1)	1.381 (14)
N(4)−N(5)	1.267 (10)	N(5)−C(6)	1.408 (13)
N(6)−C(6)	1.344 (12)	N(6)−C(10)	1.350 (13)
C(1)−C(2)	1.389 (14)	C(2)−C(3)	1.37 (2)
C(3)−C(4)	1.37 (2)	C(4)−C(5)	1.38 (2)
C(6)−C(7)	1.402 (13)	C(7)−C(8)	1.37 (2)
C(8)−C(9)	1.39 (2)	C(9)−C(10)	1.391 (14)
N(4)−Re(1)−N(1)	91.7 (3)	N(4)−Re(1)−N(3)	164.9 (3)
N(1)−Re(1)−N(3)	73.2 (3)	N(4)−Re(1)−Cl(3)	103.8 (2)
N(1)−Re(1)−Cl(3)	164.2 (2)	N(3)−Re(1)−Cl(3)	91.2 (3)
N(4)−Re(1)−Cl(2)	94.9 (3)	N(1)−Re(1)−Cl(2)	94.5 (2)
N(3)−Re(1)−Cl(2)	88.1 (2)	Cl(3)−Re(1)−Cl(2)	86.95 (9)
N(4)−Re(1)−Cl(1)	91.2 (2)	N(1)−Re(1)−Cl(1)	90.9 (2)
N(3)−Re(1)−Cl(1)	87.4 (2)	Cl(3)−Re(1)−Cl(1)	86.23 (8)
Cl(2)−Re(1)−Cl(1)	171.77 (9)	N(2)−N(1)−Re(1)	127.7 (6)
N(1)−N(2)−C(1)	109.1 (8)	C(5)−N(3)−C(1)	116.8 (9)
C(5)−N(3)−Re(1)	130.1 (8)	C(1)−N(3)−Re(1)	113.1 (6)
N(5)−N(4)−Re(1)	175.3 (7)	N(4)−N(5)−C(6)	118.7 (8)

Table 16. Selected Bond Lengths (Å) and Angles (deg) for $[ReCl_3(NNC_3H_4N_2H)(HNNHC_3H_4N_2H)]$ (**5**)

Re(1)−N(5)	1.755 (14)	Re(1)−N(1)	1.971 (14)
Re(1)−N(3)	2.067 (12)	Re(1)−Cl(2)	2.430 (4)
Re(1)−Cl(1)	2.451 (3)	Re(1)−Cl(3)	2.458 (4)
N(1)−N(2)	1.27 (2)	N(2)−C(4)	1.34 (2)
N(3)−C(4)	1.30 (2)	N(3)−C(6)	1.504 (2)
N(4)−C(4)	1.36 (2)	N(4)−C(5)	1.47 (2)
N(5)−N(6)	1.28 (2)	N(6)−C(1)	1.35 (2)
N(7)−C(1)	1.31 (2)	N(7)−C(2)	1.48 (2)
N(8)−C(1)	1.33 (2)	N(8)−C(3)	1.46 (2)
C(2)−C(3)	1.54 (2)	C(6)−C(5)	1.54 (2)
N(5)−Re(1)−N(1)	94.1(6)	N(5)−Re(1)−N(3)	167.6(6)
N(1)−Re(1)−N(3)	73.6(5)	N(5)−Re(1)−Cl(2)	93.2(5)
N(1)−Re(1)−Cl(2)	91.2(4)	N(3)−Re(1)−Cl(2)	86.0(4)
N(5)−Re(1)−Cl(1)	94.0(5)	N(1)−Re(1)−Cl(1)	95.3(4)
N(3)−Re(1)−Cl(1)	88.4(4)	Cl(2)−Re(1)−Cl(1)	169.87(12)
N(5)−Re(1)−Cl(3)	102.7(5)	N(1)−Re(1)−Cl(3)	163.0(4)
N(3)−Re(1)−Cl(3)	89.6(3)	Cl(2)−Re(1)−Cl(3)	85.17(14)
Cl(1)−Re(1)−Cl(3)	86.36(12)	N(2)−N(1)−Re(1)	123.5(11)
N(1)−N(2)−C(4)	109.8(14)	C(4)−N(3)−C(6)	110.1(10)
C(4)−N(3)−Re(1)	113.3(10)	C(6)−N(3)−Re(1)	136.6(8)
C(4)−N(4)−C(5)	107.3(14)	N(6)−N(5)−Re(1)	174.8(12)

The use of molybdate in the synthesis of **6** demonstrates that metal−oxo species other than those of group 7 can also be used in the syntheses. While preparation of molybdenum−hydrazido species is by no means novel,[21] the use of vacuum-sealed glass tubes provides a useful method for the isolation of Mo−hydrazido species. These syntheses demonstrate that metal oxides $[MO_4]^-$ react readily with chelating hydrazine ligands in a variety of solvents to give robust complexes[22] with a variety of metal−organohydrazine cores.

As noted in the structural discussion (vide infra), the $\{M(\eta^1\text{-}NNC_5H_4NH)(\eta^2\text{-}HNNH_xC_5H_4N)\}$ cores of **2**, **3**, and **6** exhibit protonated pyridine nitrogen sites for the hydrazinopyridine in the monodentate ligating mode. Deprotonation of this site could be accomplished by treatment with base to produce the anionic complex, as demonstrated by the synthesis of $[Et_3NH][ReCl_3(\eta^1\text{-}NNC_5H_4N)(\eta^2\text{-}HNNC_5H_4N)]$ (**4**):

$$[ReCl_3(\eta^1\text{-}NNC_5H_4NH)(\eta^2\text{-}HNNC_5H_4N)] + Et_3N \rightarrow [Et_3NH][ReCl_3(\eta^1\text{-}NNC_5H_4N)(\eta^2\text{-}HNNC_5H_4N)]$$
$$\mathbf{3} \qquad\qquad \mathbf{4}$$

Related organohydrazine ligands, such as 2-hydrazino-2-imidazoline $H_2NNH(C_3H_4NH)$, provide analogous compounds

Table 17. Selected Bond Lengths (Å) and Angles (deg) for $[MoCl_3(NNC_5H_4NH)(HNNHC_5H_4N)]$ (**6**)

Mo(1)−N(4)	1.761(3)	Mo(1)−N(1)	1.948(3)
Mo(1)−N(3)	2.228(3)	Mo(1)−Cl(1)	2.4273(10)
Mo(1)−Cl(2)	2.4482(10)	Mo(1)−Cl(3)	2.4930(10)
N(1)−N(2)	1.352(5)	N(2)−C(1)	1.358(6)
N(3)−C(1)	1.346(5)	N(3)−C(5)	1.351(5)
N(4)−N(5)	1.271(5)	N(5)−C(6)	1.366(5)
N(6)−C(7)	1.348(5)	N(6)−C(6)	1.352(5)
C(1)−C(2)	1.409(6)	C(2)−C(3)	1.373(7)
C(3)−C(4)	1.399(6)	C(4)−C(5)	1.370(6)
C(6)−C(10)	1.404(6)	C(7)−C(8)	1.355(6)
C(8)−C(9)	1.403(6)	C(9)−C(10)	1.380(6)
N(4)−Mo(1)−N(1)	93.2(2)	N(4)−Mo(1)−N(3)	166.81(14)
N(1)−Mo(1)−N(3)	74.06(13)	N(4)−Mo(1)−Cl(1)	100.31(11)
N(1)−Mo(1)−Cl(1)	94.41(10)	N(3)−Mo(1)−Cl(1)	84.42(8)
N(4)−Mo(1)−Cl(2)	93.32(11)	N(3)−Mo(1)−Cl(2)	92.70(10)
N(3)−Mo(1)−Cl(2)	84.03(8)	Cl(1)−Mo(1)−Cl(2)	164.23(4)
N(4)−Mo(1)−Cl(3)	96.71(11)	N(1)−Mo(1)−Cl(3)	170.03(11)
N(3)−Mo(1)−Cl(3)	95.98(8)	Cl(1)−Mo(1)−Cl(3)	84.83(3)
Cl(2)−Mo(1)−Cl(3)	85.73(3)	N(2)−N(1)−Mo(1)	121.9(3)
N(1)−N(2)−C(1)	116.4(3)	C(1)−N(3)−C(5)	118.3(3)
C(1)−N(3)−Mo(1)	112.8(3)	C(5)−N(3)−Mo(1)	128.9(2)
N(5)−N(4)−Mo(1)	170.0(3)	N(4)−N(5)−C(6)	115.9(3)

Table 18. Selected Bond Lengths (Å) and Angles (deg) for $[Tc(C_5H_4NS)_2(NNC_5H_4N)(HNNC_5H_4N)]$ (**7**)

Tc(1)−S(1)	2.489(3)	Tc(1)−S(2)	2.408(3)
Tc(1)−N(1)	1.985(9)	Tc(1)−N(3)	2.150(7)
Tc(1)−N(4)	1.767(9)	Tc(1)−N(7)	2.144(9)
S(1)−C(11)	1.758(10)	S(2)−C(16)	1.794(11)
N(1)−N(2)	1.340(14)	N(2)−C(1)	1.384(14)
N(3)−C(1)	1.360(16)	N(3)−C(5)	1.346(14)
N(4)−N(5)	1.237(13)	N(5)−C(6)	1.395(14)
N(6)−C(6)	1.335(14)	N(6)−C(7)	1.333(15)
N(7)−C(11)	1.346(13)	N(7)−C(15)	1.373(13)
N(8)−C(16)	1.326(14)	N(8)−C(20)	1.351(18)
C(1)−C(2)	1.403(16)	C(2)−C(3)	1.358(17)
C(3)−C(4)	1.396(18)	C(4)−C(5)	1.358(16)
C(6)−C(10)	1.371(16)	C(7)−C(8)	1.368(19)
C(8)−C(9)	1.402(23)	C(9)−C(10)	1.357(22)
C(11)−C(12)	1.382(16)	C(12)−C(13)	1.393(17)
C(13)−C(14)	1.414(18)	C(14)−C(15)	1.380(17)
C(16)−C(17)	1.383(16)	C(17)−C(18)	1.389(18)
C(18)−C(19)	1.380(23)	C(19)−C(20)	1.329(22)
S(1)−Tc(1)−S(2)	156.1(1)	S(1)−Tc(1)−N(1)	100.6 (3)
S(2)−Tc(1)−N(1)	99.9(3)	S(1)−Tc(1)−N(3)	89.8 (3)
S(2)−Tc(1)−N(3)	83.9(2)	N(1)−Tc(1)−N(3)	74.5(4)
S(1)−Tc(1)−N(4)	96.6(3)	S(2)−Tc(1)−N(4)	95.5(3)
N(1)−Tc(1)−N(4)	89.8(4)	N(3)−Tc(1)−N(4)	164.0(4)
S(1)−Tc(1)−N(7)	66.1(2)	S(2)−Tc(1)−N(7)	90.9(2)
N(1)−Tc(1)−N(7)	161.0(4)	N(3)−Tc(1)−N(7)	91.3(4)
N(4)−Tc(1)−N(7)	104.7(4)	Tc(1)−S(1)−C(11)	80.3(4)
Tc(1)−S(2)−C(16)	109.2(3)	Tc(1)−N(1)−N(2)	123.4(7)
N(1)−N(2)−C(1)	111.2(9)	Tc(1)−N(3)−C(1)	112.8(7)
Tc(1)−N(3)−C(5)	128.7(8)	C(1)−N(3)−C(5)	118.4(8)
Tc(1)−N(4)−N(5)	175.1(8)	N(4)−N(5)−C(6)	123.5(9)
C(6)−N(6)−C(7)	116.4(10)	Tc(1)−N(7)−C(11)	104.1(7)
Tc(1)−N(7)−C(15)	136.4(7)	C(11)−N(7)−C(15)	119.5(9)

(21) (a) Crichton, B. A. L.; Dilworth, J. R.; Dahlstrom, P.; Zubieta, J. *Transition Met. Chem. (London)* **1980**, *5*, 316−317. (b) Chatt, J.; Crichton, B. A. L.; Dilworth, J. R.; Dahlstrom, P.; Gutkoska, R.; Zubieta, J. *Inorg. Chem.* **1982**, *21*, 2383. (c) Burt, R. J.; Dilworth, J. R.; Leigh, G. J.; Zubieta, J. A. *J. Chem. Soc., Dalton Trans.* **1982**, 2295. (d) Chatt, J.; Crichton, B. A. L.; Dilworth, J. R.; Dahlstrom, P.; Gutkoska, R.; Zubieta, J. A. *Transition Met. Chem. (London)* **1979**, *4*, 11. (e) FitzRoy, M. D.; Frederiksen, J. M.; Murray, K. S.; Snow, M. R. *Inorg. Chem.* **1985**, *24*, 3265.

(22) No decomposition was observed by IR when **9** was stirred in 10:90 H_2O/CH_3CN for 1 week.

Table 19. Selected Bond Lengths (Å) and Angles (deg) for $[Re(C_5H_4NS)_2(NNC_5H_4N)(HNNC_5H_4N)]$ (**8**)

Re(1)−S(1)	2.478(2)	Re(1)−S(2)	2.392(1)
Re(1)−N(1)	1.952(5)	Re(1)−N(3)	2.125(4)
Re(1)−N(4)	1.766(5)	Re(1)−N(7)	2.169(5)
S(1)−C(11)	1.758(6)	S(2)−C(16)	1.780(6)
N(1)−N(2)	1.323(8)	N(2)−C(1)	1.357(8)
N(3)−C(1)	1.369(10)	N(3)−C(5)	1.369(9)
N(4)−N(5)	1.237(7)	N(5)−C(6)	1.398(8)
N(6)−C(6)	1.337(8)	N(6)−C(7)	1.349(9)
N(7)−C(11)	1.327(7)	N(7)−C(15)	1.351(7)
N(8)−C(16)	1.347(8)	N(8)−C(20)	1.344(10)
C(1)−C(2)	1.415(9)	C(2)−C(3)	1.369(10)
C(3)−C(4)	1.394(10)	C(4)−C(5)	1.365(10)
C(6)−C(10)	1.396(10)	C(7)−C(8)	1.375(11)
C(8)−C(9)	1.403(13)	C(9)−C(10)	1.371(12)
C(11)−C(12)	1.392(9)	C(12)−C(13)	1.371(10)
C(13)−C(14)	1.386(11)	C(14)−C(15)	1.365(9)
C(16)−C(17)	1.382(9)	C(17)−C(18)	1.400(10)
C(18)−C(19)	1.370(14)	C(19)−C(20)	1.380(13)
S(1)−Re(1)−S(2)	154.6(1)	S(1)−Re(1)−N(1)	99.8(1)
S(2)−Re(1)−N(1)	101.9(1)	S(1)−Re(1)−N(3)	89.9(2)
S(2)−Re(1)−N(3)	83.8(1)	N(1)−Re(1)−N(3)	73.3(3)
S(1)−Re(1)−N(4)	96.7(1)	S(2)−Re(1)−N(4)	96.1(1)
N(1)−Re(1)−N(4)	90.8(2)	N(3)−Re(1)−N(4)	163.6(3)
S(1)−Re(1)−N(7)	66.0(1)	S(2)−Re(1)−N(7)	89.6(1)
N(1)−Re(1)−N(7)	159.7(2)	N(3)−Re(1)−N(7)	91.6(3)
N(4)−Re(1)−N(7)	104.7(2)	Re(1)−S(1)−C(11)	80.4(2)
Re(1)−S(2)−C(16)	108.9(2)	Re(1)−N(1)−N(2)	126.1(4)
N(1)−N(2)−C(1)	109.8(5)	Re(1)−N(3)−C(1)	113.3(5)
Re(1)−N(3)−C(5)	128.7(5)	C(1)−N(3)−C(5)	118.0(5)
Re(1)−N(4)−N(5)	176.2(4)	N(4)−N(5)−C(6)	121.1(5)
C(6)−N(6)−C(7)	116.1(6)	Re(1)−N(7)−C(11)	103.3(4)
Re(1)−N(7)−C(15)	136.6(4)	C(11)−N(7)−C(15)	120.1(5)

Table 20. Selected Bond Lengths and Angles for $[Re(C_4H_3N_2S)_2(NNC_5H_4N)(HNNC_5H_4N)]$ (**9**)

Re(1)−N(4)	1.71(2)	Re(1)−N(1)	1.95(2)
Re(1)−N(3)	2.12(2)	Re(1)−N(9)	2.16(2)
Re(1)−S(2)	2.402(7)	Re(1)−S(1)	2.482(8)
S(1)−C(15)	1.74(3)	S(2)−C(11)	1.80(3)
N(1)−N(2)	1.33(3)	N(2)−C(1)	1.39(3)
N(3)−C(1)	1.36(4)	N(3)−C(2)	1.37(4)
N(4)−N(5)	1.29(3)	N(5)−C(6)	1.44(4)
N(6)−C(6)	1.31(3)	N(6)−C(10)	1.35(4)
N(7)−C(14)	1.32(4)	N(7)−C(11)	1.35(4)
N(8)−C(11)	1.43(5)	N(8)−C(12)	1.45(3)
N(9)−C(18)	1.40(3)	N(9)−C(15)	1.40(3)
N(10)−C(15)	1.30(3)	N(10)−C(16)	1.31(4)
C(1)−C(5)	1.42(4)	C(2)−C(3)	1.37(4)
C(3)−C(4)	1.33(4)	C(4)−C(5)	1.39(4)
C(6)−C(7)	1.37(4)	C(7)−C(8)	1.33(4)
C(8)−C(9)	1.36(4)	C(9)−C(10)	1.37(4)
C(12)−C(13)	1.27(4)	C(13)−C(14)	1.47(4)
C(16)−C(17)	1.40(5)	C(17)−C(18)	1.31(4)
N(4)−Re(1)−N(1)	90.7(10)	N(4)−Re(1)−N(3)	164.7(12)
N(1)−Re(1)−N(3)	74.3(12)	N(4)−Re(1)−N(9)	105.6(9)
N(1)−Re(1)−N(9)	158.8(9)	N(3)−Re(1)−N(9)	89.7(13)
N(4)−Re(1)−S(2)	96.8(8)	N(1)−Re(1)−S(2)	102.1(8)
N(3)−Re(1)−S(2)	83.4(6)	N(9)−Re(1)−S(2)	89.5(6)
N(4)−Re(1)−S(1)	95.8(8)	N(1)−Re(1)−S(1)	99.4(7)
N(3)−Re(1)−S(1)	90.1(8)	N(9)−Re(1)−S(1)	66.2(6)
S(2)−Re(1)−S(1)	154.9(2)	C(15)−S(1)−Re(1)	82.3(9)
C(11)−S(2)−Re(1)	106.1(10)	N(2)−N(1)−Re(1)	125(2)
N(1)−N(2)−C(1)	110(2)	C(1)−N(3)−C(2)	118(2)
C(1)−N(3)−Re(1)	114(2)	C(2)−N(3)−Re(1)	129(3)
N(5)−N(4)−Re(1)	176(2)	N(4)−N(5)−C(6)	118(2)

upon reaction with metal oxides. Thus, the reaction of $[ReO_4]^-$ with 2-hydrazino-2-imidazoline yields $[ReCl_3(NNC_3H_4N_2H)(HNNHC_3H_4N_2H)]$ (**5**), a complex whose $\{Re(\eta^1\text{-NNR})(\eta^2\text{-HNNHR})\}$ core is a variant of that observed for **3**, but analogous to that of **6**, as discussed in the structural description of these complexes (vide infra). This structural modification appears

Table 21. Selected Bond Lengths and Angles for $[Mo(C_4H_3N_2S)_3(NNC_5H_4N)]$ (**12**)

Mo(1)−N(1)	1.797 (3)	Mo(1)−N(8)	2.190 (3)
Mo(1)−N(6)	2.204 (3)	Mo(1)−N(4)	2.227 (3)
Mo(1)−S(1)	2.4826 (9)	Mo(1)−S(2)	2.5232 (9)
Mo(1)−S(3)	2.5306 (10)	S(1)−C(6)	1.738 (4)
S(2)−C(10)	1.734 (4)	S(3)−C(14)	1.739 (4)
N(1)−N(2)	1.234 (4)	N(2)−C(1)	1.438 (5)
N(3)−C(1)	1.328 (5)	N(3)−C(5)	1.338 (6)
N(4)−C(9)	1.337 (5)	N(4)−C(6)	1.369 (5)
N(5)−C(6)	1.326 (5)	N(5)−C(7)	1.345 (6)
N(6)−C(11)	1.336 (5)	N(6)−C(10)	1.353 (5)
N(7)−C(10)	1.325 (5)	N(7)−C(13)	1.329 (6)
N(8)−C(17)	1.341 (5)	N(8)−C(14)	1.347 (5)
N(9)−C(14)	1.315 (5)	N(9)−C(15)	1.340 (6)
C(1)−C(2)	1.377 (6)	C(2)−C(3)	1.385 (7)
C(3)−C(4)	1.372 (7)	C(4)−C(5)	1.361 (7)
C(7)−C(8)	1.370 (7)	C(8)−C(9)	1.368 (6)
C(11)−C(12)	1.378 (6)	C(12)−C(13)	1.364 (7)
C(15)−C(16)	1.375 (7)	C(16)−C(17)	1.378 (6)
N(1)−Mo(1)−N(S)	88.54(12)	N(1)−Mo(1)−N(6)	86.08(12)
N(8)−Mo(1)−N(6)	159.09(11)	N(1)−Mo(1)−N(4)	165.07(12)
N(8)−Mo(1)−N(4)	88.77(11)	N(6)−Mo(1)−N(4)	91.24(11)
N(1)−Mo(1)−S(1)	99.44(9)	N(8)−Mo(1)−S(1)	80.97(8)
N(6)−Mo(1)−S(1)	80.01(8)	N(4)−Mo(1)−S(1)	65.63(8)
N(1)−Mo(1)−S(2)	101.37(9)	N(8)−Mo(1)−S(2)	137.09(8)
N(6)−Mo(1)−S(2)	63.82(8)	N(4)−Mo(1)−S(2)	90.54(8)
S(1)−Mo(1)−S(2)	136.41(3)	N(1)−Mo(1)−S(3)	105.72(10)
N(8)−Mo(1)−S(3)	63.76(8)	N(6)−Mo(1)−S(3)	137.10(8)
N(4)−Mo(1)−S(3)	86.18(8)	S(1)−Mo(1)−S(3)	135.38(3)
S(2)−Mo(1)−S(3)	73.38(3)	C(6)−S(1)−Mo(1)	82.39(13)
C(10)−S(2)−Mo(1)	82.59(12)	C(14)−S(3)−Mo(1)	82.14(13)
N(2)−N(1)−Mo(1)	174.5(3)	N(1)−N(2)−C(1)	118.4(3)

to reflect the reduced basicity of imidazole with respect to pyridine, whose pK_b values are approximately 6.92 and 5.25, respectively. Consequently, protonation of the second imidazole ring nitrogen to produce an imidazolium diazenido species analogous to the pyridinium diazenido group (vide infra, Figure 6B) is unlikely. Preferential protonation at the β-nitrogen site of the hydrazine moiety results in the observed structure and establishes the relative proton affinities of these two sites. Chelated organohydrazine ligands have been described previously for the N,O-coordinated benzoylhydrazine-containing complexes.[23] In contrast to these latter complexes that involve substitutionally inert, biologically irrelevant triphenylphosphine coligands, the complexes **2**−**6** presented in this work[24] have only labile chlorine coligands that are readily substituted by a variety of ligand types, most notably members of the pyridinethiol and pyrimidinethiol families.

The ^{1}H NMR spectra of **3** and **4**, shown in Figure 4, illustrate the predicted splitting patterns for the hydrazido aromatic ring. The exchangeable protons in **3**, both the α-nitrogen proton and *N*-pyridyl proton, appear at 4.22 ppm, which suggests some interconversion or equilibration in solution. The spectra also allow for tentative assignment of the α-nitrogen proton for **4** at 8.2 ppm.

The IR spectra of **2**, **3**, **5**, and **6** display a strong band in the 1560−1522 cm^{-1} region assigned to ν(N═N), suggesting that these compounds exhibit comparable ligand multiple bonding character despite variations in metal and organohydrazine type. The remainder of the IR spectra in the 500−3000 cm^{-1} range

(23) Chatt, J.; Dilworth, J. R.; Leigh, G. L. *J. Chem. Soc., Dalton Trans.* **1973**, 612.

(24) (a) McClevery, J. A.; Seddon, D.; Whitely, R. N. *J. Chem. Soc., Dalton Trans.* **1975**, 839. (b) Carroll, W. E.; Deare, M. E.; Labor, F. J. *J. Chem. Soc., Dalton Trans.* **1974**, 1837. (c) Chatt, J.; Dilworth, J. R.; Leigh, G. J. *J. Chem. Soc., Dalton Trans.* **1979**, 1843. (d) Colin, J. Butler, G.; Weiss, J. *Inorg. Chem.* **1980**, *45*, 3828.

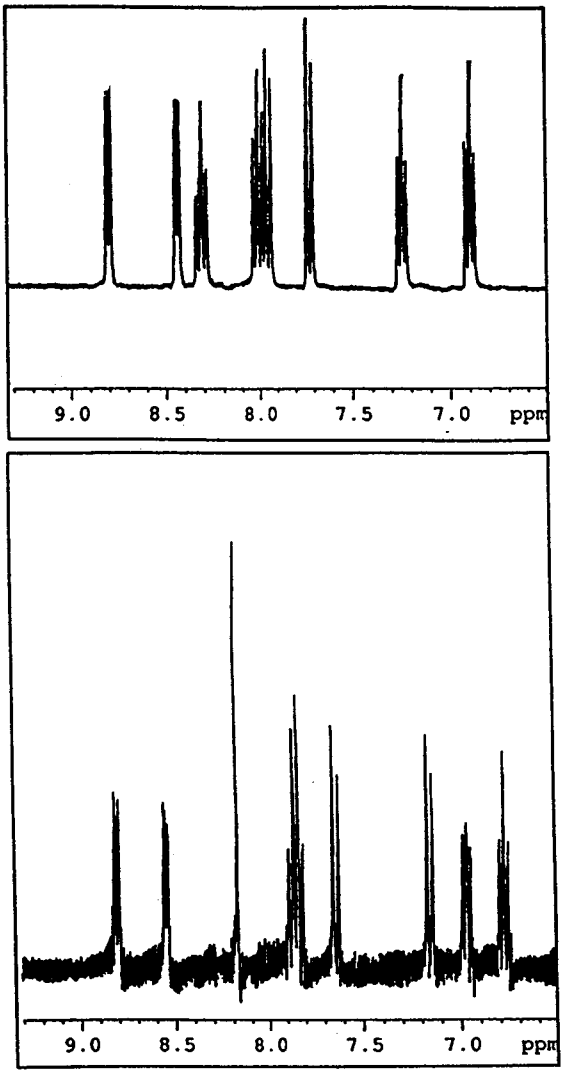

Figure 4. Aromatic region ^{1}H NMR of $[ReCl_3(NNC_5H_4NH)(HNNC_5H_4N)]$ (**3**) (top) and $[HNEt_3][ReCl_3(\eta^1\text{-}NNC_5H_5N)(\eta^2\text{-}HNNC_5H_4N)]\cdot H_2O$ (**4**) (bottom).

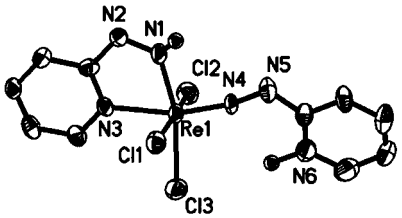

Figure 5. View of the structure of **3**, showing the atom-labeling scheme and the 50% thermal ellipsoid probabilities.

are dominated by modes associated with the organic framework of the ligands.

The coligands of interest for this study are pyrimidinethiols and pyridinethiols of Scheme 3 which have been found to influence the biodistribution patterns of the ^{99m}Tc-labeled peptides. Metal complexes of thiolate ligands with nitrogen-containing aromatic residues are preferred for their ease of preparation, facility of substitution, high yield, and ready isolation. The reactions of the complexes with the $\{M(\eta^1\text{-}NNC_5H_4NH)(\eta^2\text{-}HNNC_5H_4N)\}$ cores, **2** and **3**, with pyridine-2-thiol yield compounds of the general class $[M(C_5H_4NS)_2(\eta^1\text{-}NNC_5H_4N)(\eta^2\text{-}HNNC_5H_4N)]$ (M = Tc (**7**), Re (**8**)). Both reactions require base to deprotonate the pyridine nitrogen site, providing in situ formation of species similar to **4**, $[HNEt_3][MCl_3(\eta^1\text{-}NNC_5H_4N)(\eta^2\text{-}NHNC_5H_4N)]$, which subsequently undergo chloride ligand substitution.

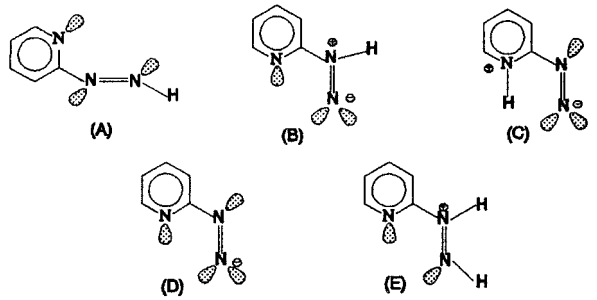

Figure 6. Structural modes adopted by organohydrazines in their coordination chemistry, as discussed in the text.

The syntheses of the pyrimidine-2-thiol containing complexes $[Re(C_4H_3N_2S)_2(NNC_5H_4N)(HNNC_5H_4N)]$ (**9**), $[Mo(C_4H_3N_2S)_2(NNC_5H_4N)(HNNHC_5H_4N)]$ (**11**), and $[Mo(C_4H_3N_2S)_3(NNC_5H_4N)]$ (**12**) proceed similarly to those of the pyridine-2-thiol derivatives **7** and **8**. While rhenium exhibits only a bis-pyrimidinethiolate complex, it is noteworthy that molybdenum yields both bis- and tris-pyrimidinethiolato complexes, **11** and **12**, respectively. The presence of both **11** and **12** as a mixed product in the synthesis suggests that several species may be present in medicinal preparations at the tracer level. Although a seven-coordinate thiolate complex of rhenium has been prepared previously,[18] no analogous seven-coordinate hydrazido−thiolate−rhenium or technetium species have been detected in this work. Compounds **11** and **12** may be separated quite readily by exploiting solubility differences in organic solvents.

An analogous quinoline-2-thiol derivative $[Re(C_9H_6NS)(NNC_5H_4N)(HNNC_5H_4N)]$ (**10**) was prepared in a similar fashion from the reaction of **3** with quinoline-2-thiol in ethanol in the presence of triethylamine. Curiously, Tc−organohydrazine species have been observed to undergo N−N bond cleavage in the presence of quinolinethiols to give Tc−nitrido complexes such as $[TcN(C_9H_6NS)_2]$.[25] It is noteworthy that 8-quinolinol complexes of ^{99m}Tc show promise as brain-uptake or as blood-labeling agents.[26]

Characterization of the metal−organohydrazine−thiolate class of compounds, **7**−**12**, was accomplished by elemental analysis and infrared spectroscopy, as well as X-ray crystallography. As a consequence of the poor solubility of the compounds in most solvents, the ^{1}H NMR spectra of these species provided limited structural information, consisting of a complex pattern of multiplets in the aromatic region. This may suggest that the thiolate ligands are fluctional in solution. The IR spectra of **7**−**12** display bands characteristic both of the aromatic thiolate ligands and of the organohydrazine ligand. In addition to the characteristic organohydrazido bands between 1560 and 1522 cm^{-1} assigned to ν(N═N), the spectra contain a series of bands in the 1430−1630 cm^{-1} range attributed to aromatic thiolate ring stretching modes ν(C═C) and ν(C═N).

The chloride ligands of the $[MCl_3(NNR)(HNNR)]$ class of complexes are readily displaced by ligands other than S- or S,N-donating pyridinethiol and pyrimidinethiol types. For example, **3** reacts with 3,4-dihydroxybenzoate and PPh_3 to give $[Re(C_8H_6O_4)(PPh_3)(NNC_5H_4N)]$ (**13**). The ^{31}P NMR spectrum of **13** exhibits a single peak at 21.48 ppm, characteristic of such

(25) Dilworth, J. R. *Coord. Chem. Rev.* **1996**, *154*, 163−177 and references therein.
(26) Loberg, M. P.; Corder, E. H.; Fields, A. I.; Callery, P. S. *J. Nucl. Med.* **1979**, *20*, 1181.

complexes, while the typical infrared bands associated with the ν(N═N) appear in the 1470−1560 cm^{-1} range. Such catechol complexes may be of general interest in view of the biological activity associated with catechol complexes in general and the interaction of catechol-derivatized imidazoles with α-adrenoceptors.[27]

The observation that the use of D-mannitol in the preparation of technetium−organohydrazino−proteins conjugates provides products with useful biodistribution suggested the preparation of [Re($C_6H_{12}O_6$)(η^1-NNC_5H_4N)(η^2-$NHNC_5H_4N$)] (**14**),[5b] a complex synthesized by reacting **3** with D-mannitol in ethanol in the presence of base. Attempts to crystallize such {metal−organohydrazido−sugar} species as models for the compounds employed in biodistribution studies have been unsuccessful to date. The crude product from the synthesis of **14** appears to contain several species with different solubilities: a water-soluble fraction, which analyzes as a complex mixture, and a water-insoluble fraction (**14**).

Such complex solution behavior correlates with the observation that the {^{99m}Tc−(mannitol)−HYNIC−peptide} conjugates have multiple peaks in the HPLC. However, refluxing **14** with pyridine-2-thiol in ethanol in the presence of triethylamine produced a single compound, [Re(C_5H_4NS)$_2$(NNC_5H_3N)-($HNNC_5H_3N$)] (**8**), in good yield. Attempts at isolating the mixed ligand [Re(mannitol)(C_5H_4NS)$_2$($H_xNNC_5H_3N$)$_2$] complex by limiting the amount of pyridine-2-thiol resulted in the isolation of a mixture of **8** and **14**.

These observations suggest some analogies to the radiolabeled HYNIC−protein conjugates. Preparation of radiolabled HYNIC−protein conjugate starts with reduced {^{99m}Tc−(D-mannitol)} providing the necessary Tc(V)−oxo species, which is then reacted with the HYNIC−protein conjugate. Previous studies have demonstrated that the {^{99m}Tc−(D-mannitol)−HYNIC−protein} conjugate gave superior imaging results when compared to other polyhydridic "coligands". Radio-HPLC also indicated the presence of several {^{99m}Tc−(D-mannitol)−HYNIC−protein} conjugate species. Reaction of {^{99m}Tc−(D-mannitol)−HYNIC−protein} conjugate with pyrimidinethiols allowed the isolation of a unique hydrophobic species, which has been shown to offer excellent infection localization but with some gastrointestinal tract accumulation. Curiously, the pyridinethiols did not perform well as conjugate "coligands".

The differences in biodistribution of pyridine-2-thiol and pyrimidine-2-thiol ^{99m}Tc complexes have also been observed for technetium nitride, {Tc(N)}, and tin-reduced technetium, {Tc(Sn)}.[28] {^{99m}Tc(N)−mercaptopyrimidine} had high blood activity with high lung uptake but low liver and intestinal activity while {^{99m}Tc(N)−mercaptopyridine} was not prepared in a form satisfactory for animal studies. {^{99m}Tc(Sn)−mercaptopyrimidine}[29] had low blood activity with high liver activity while {^{99m}Tc(Sn)−mercaptopyridine}[30] had hepatobiliary activity with low urinary excretion and slow liver clearance, which suggested colloidal formation in vivo.

Additionally, significant differences have been observed between pyrimidine-2-thione and pyrimidin-2-one with Tc(III).[31] When {Tc(III)−thiourea} complexes were reacted with pyrimidine-2-thione derivatives, more than 95% of the technetium was extracted into the organic phase, but hardly any was extracted with pyrimidin-2-one derivatives.

X-ray Crystallography. The structural chemistry of two families of metal−(bis)organohydrazine complexes has been addressed: (i) the trihalides of general type [MCl_3(η^1-$NNRH_x$)-(η^2-$HNNH_yR$)] (x = 0, 1; y = 0, 1) and (ii) the thiolate-containing complexes [M(η^1-SR′N)(η^2-SR′N)(η^1-NNR)(η^2-HNNR)]. While the metal−(bis)organohydrazine core provides the fundamental structural motif for the complexes of these families, the detailed geometries associated with these cores reflect the steric and electronic requirements of the metals.

As shown in Figure 5, [$ReCl_3$(η^1-NNC_5H_4NH)(η^2-HNN-C_5H_4N)] (**3**) exhibits distorted octahedral geometry, defined by three chloride ligands, the α-nitrogen of a monodentate pyridinium−diazenido ligand, and the α-nitrogen and pyridine nitrogen of a chelating organodiazene ligand. The metrical parameters for the {Re(NNR)(HNNR)} moiety are unexceptional, as suggested by the data of Table 22 comparing metal−organohydrazine cores of selected representative complexes. The singly bent {Re(η^1-NNC_5H_4NH)} grouping exhibits the characteristically short Re−N and N−N distances, with an essentially linear valence angle at N4. The {Re(η^2-$HNNC_5H_4N$)} moiety is planar and exhibits a short Re−N1 bond length, consistent with sp^2 hybridization at N1 and some multiple-bond character, while the Re−N3 distance is significantly elongated to 2.165(7) Å as a consequence of the strong trans influence of the pyridinium−diazenido linkage. The cis orientation of N1 and N4 allows full participation of the metal t_{2g}-type orbitals in π-bonding to the α-nitrogen atoms of the ligands. Another noteworthy feature of the structure is the geometry of the {Re-(η^1-NNC_5H_4NH)(η^2-$HNNC_5H_4N$)} grouping, with the ring of the pyridinium−diazenido group bent away from the Re−N1 vector and directed toward the Re−Cl3 vector.

The positions of nitrogen-bound hydrogen atoms of the organohydrazine ligands were unambiguously identified in the X-ray structure of **3** as the pyridine nitrogen of the monodentate pyridinium−diazenido ligand and the α-nitrogen of the chelating organodiazene group. The orientation of the protonated pyridyl ring with respect to the chelating organodiazene ligand appears to reflect a steric influence as placing the ring in the ReN1N4 plane adjacent to the Re−N1 vector would bring the N6 and N1 hydrogen sites into contact.

It is instructive to digress from the structural descriptions to comment on the formalisms adopted to describe the organohy-

(27) Miller, D. D.; Hamada, A.; Clark, M. T.; Adejare, A.; Patil, P. N.; Shams, G.; Romstedt, K. J.; Kim, S. U.; Intrasuksri, U.; McKenzie, J. L.; Feller, D. R. *J. Med. Chem.* **1990**, *33*, 1138−1144.

(28) Ballas, J.; Bonnyman, *J. Nucl. Med. Biol., Part B* **1988**, *15* (4), 451−457.

(29) Reduction of NH_4ReO_4 with Sn(II) in aqueous solution in the presence of excess pyrimidine-2-thiol produces [$ReO(C_4H_3N_2S)_3$] in 51% yield. The complex [$ReO(C_4H_3N_2S)_3$] has previously been reported in ref 18.

(30) Reduction of NH_4ReO_4 with Sn(II) in aqueous solution in the presence of excess pyridine-2-thiol produces a brown water-soluble compound that we have been unable to crystallize.

(31) Hashimoto, K.; Kudo, H.; Omori, T.; Yoshihara, K. *Radiochim. Acta* **1993**, *63*, 167−171.

(32) Butler, G.: Chatt, J.; Hussein, W.; Leigh, G. J.; Hugh, D. L. *Inorg. Chim. Acta* **1978**, *28*, L165.

(33) Butler, G.; Chatt, J.; Hussein, W.; Leigh, G. J.; Hughes, D. L. *Inorg. Chim. Acta* **1978**, *30*, L287.

(34) (a) Deutsch, E.; Libson, K.; Vanderheyden, J.-L.; Ketring, A. R.; Maxon, H. P. *Nucl. Med. Biol.* **1986,** *13*, 465. (b) Ehrhardt, J.; Ketring, A. R.; Turpin, T. A.; Razavi, M.-S.; Vanderheyden, J.-L.; Su, F.-M.; Fritzberg, A. R. In *Technetium and Rhenium in Chemistry and Nuclear Medicine 3*; Nicollini, M., Bandoli, G., Mazzi, U., Eds.; Cortina International: Verona, 1990; p 631. (c) Häfeli, U.; Tiefenance, L.; Schuberger, P. A. *Ibid.*; p 643. (d) Nosco, D. L.; Tofe, A. J.; Dunn, T. J.; Lyle, L. R.; Wolfangel, R. G.; Bushman, M. J.; Grummon, G. D.; Helling, D. E.; Marmion, M. E.; Milles, K. M.; Pipes, D. W.; Saubel, T. W.; Webster, D. W. *Ibid.*; p 381. (e) Maxon, H. R., III; Schroder, L. E.; Thomas, S. R.; Hertzberg, V. S.; Deutsch, E.; Samotunga, R. C.; Libson, K.; Williams, C. C.; Maulton, J. S.; Schneider, H. J. *Ibid.*; p 733.

(35) Vanderheyden, J.-L.; Heeg, M. J.; Deutsch, E. *Inorg. Chem.* **1988**, *27*, 1666.

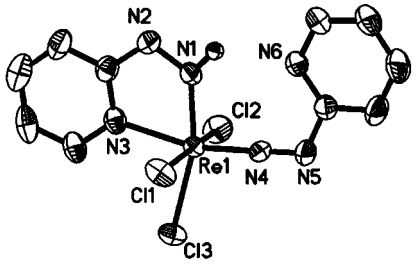

Figure 7. View of the structure of the anion of **4**, showing the atom-labeling scheme and 50% thermal ellipsoid probabilities.

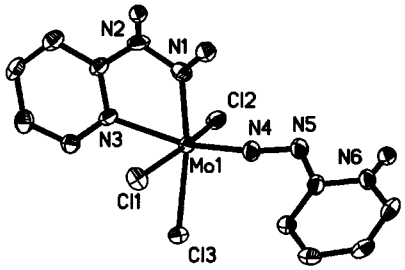

Figure 8. View of the structure of **6**, showing the atom-labeling scheme and 50% thermal ellipsoid probabilities.

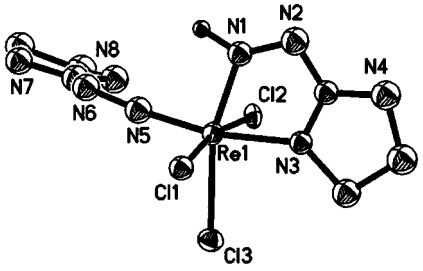

Figure 9. ORTEP view of the structure of **5**, showing the atom-labeling scheme and 50% thermal ellipsoid probabilities.

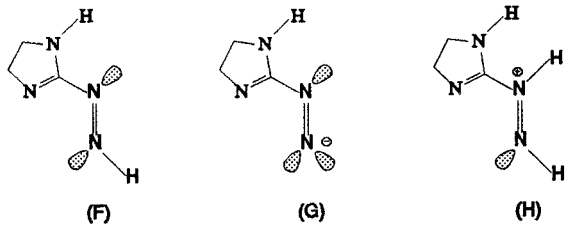

Figure 10. Potential coordination modes for the imidazole−hydrazine ligand (F), as discussed in the text.

drazine ligation modes. As we have previously noted,[36ag] the ligands are best described as formally derived from neutral organodiazene, RN═NH, rather than as deprotonated organohydrazines, H_2NNHR. The organodiazene formalism conforms more realistically to the metrical parameters associated with the metal−ligand coordination geometries and with the hybridization scheme invoked to rationalize the bonding. Thus, as illustrated in Figure 6, the organohydrazine ligands may be present as the neutral organodiazene (A), the neutral zwitterionic "hydrazido(2−)" (B), the neutral pyridinium−diazenido group (C), the mononegative anionic organodiazenido(1−) ligand (D), or the monopositive cationic organohydrazinium unit (E). While this formalism is somewhat arbitrary, it does possess the advantages of deriving from a realistic picture of the bonding in the complexes and of providing a self-consistent scheme for the various ligation modes adopted by the complexes of this study. Specifically complexes **2**−**12** are diamagnetic, a characteristic consistent with the formalism adopted. Thus, compound **3** is formally a Re(III) species with a d^4 electronic configuration, consistent with diamagnetic behavior.

Deprotonation of **3** results in the isolation of $[Et_3NH][ReCl_3(\eta^1\text{-}NNC_5H_4N)(\eta^2\text{-}HNNC_5H_4N)]$ (**4**). As shown in Figure 7, the structure of **4** is grossly similar to that of **3** in

exhibiting a distorted octahedral $\{ReN_3Cl_3\}$ coordination environment with a planar $\{Re(NNC_5H_4N)(HNNC_5H_4N)\}$ unit. The metrical parameters within this unit are similar to those of **3**. However, it is noteworthy that pyridine nitrogen N6 has been deprotonated, resulting in a reorientation of the pyridyl group of the pyridyldiazenido(1−) ligand adjacent to the Re−N1 bond vector. The structure of **4** unambiguously identifies N1 as the hydrogen-bound site, and the proximity of N6···N1(H1) suggests weak hydrogen bonding between these sites. A similar ring "flip" was described previously for the structure of $[ReCl_2(PPh_3)(\eta^1\text{-}NNC_5H_4N)(\eta^2\text{-}HNNC_5H_4N)]$, which also exhibits a monodentate pyridyldiazenido(1−) ligand and a chelating pyridyldiazene group.[34a]

Compounds **5** and **6** exhibit yet a third orientation of the organohydrazine ligands, as shown in Figures 8 and 9. The molybdenum derivative $[MoCl_3(\eta^1\text{-}NNC_5H_4NH)(\eta^2\text{-}HNNHC_5H_4N)]$ (**6**) exhibits the distorted $\{MoCl_3N_3\}$ core, analogous to those of **3** and **4**. While the metrical parameters associated with the $[Mo(NNC_5H_4NH)(HNNHC_5H_4N)]$ unit of **6** are similar to those observed for **3** and **4**, the relative orientation of the pyridyl group of the pyridinium−diazenido ligand with respect to the metal-chelating pyridyldiazene unit is distinct. Rather than sitting in the {MoN1N4} plane, the ring is normal to the plane and parallel to the Cl2−Mo−Cl3 vector.

Another noteworthy distinction associated with the structure of **6** is the protonation of the β-nitrogen site of the chelating organohydrazine ligand. The organohydrazine groups are thus formally described as the monodentate pyridinium−diazenido ligand and the chelating pyridylhydrazinium(1+) group, $(\eta^2\text{-}HNNHC_5H_4N)^+$. Thus, the molybdenum site is formally Mo(II), consistent with the observed diamagnetism. It would appear that the coordination modalities adopted by the organohydrazine ligands are sensitive to the electronic requirements of the metal center.

Substitution of the pyridyl unit by other potentially ligating functionalities, such as the imidazole group, may be effected to give analogous structural types, as represented by $[ReCl_3(\eta^1\text{-}NNC_3H_4N_2H)(\eta^2\text{-}HNNHC_3H_4N_2H)]$ (**5**). As illustrated in Figure 10, compound **5** adopts the same relative orientations of imidazole−hydrazine rings as previously described for **6**, consistent with the formulation of the monodentate group as the imidazole−diazenido(1−) unit (G), with hydrogen bonded to N7, and the chelating ligand as the monopositive imidazole hydrazinium(1+) group (H), with N−H bonds at N1, N2, and N4. As noted previously, the relatively low proton affinity of the imidazole precludes protonation at the N8 site to form the imidazolium−diazenido species analogous to the pyridinium−diazenido group observed in the structures of **3** and **6**. As in the case of **6**, the relative orientation of organohydrazine rings

(36) (a) Nicholson, T.; Cook, J.; Davison, A.; Rose, D. J.; Maresca, K. P.; Zubieta, J.; Jones, A. G. *Inorg. Chim. Acta* **1996**, *252*, 427−430. (b) Nicholson, T.; de Vries, N.; Davison, A.; Jones, A. G. *Inorg. Chem.* **1989**, *28*, 3813−3819. (c) Abrams, M. J.; Larsen, S. K.; Shaikh, S. N.; Zubieta, J. *Inorg. Chim. Acta* **1991**, *185*, 7−15. (d) Nicholson, T.; Lombardi, P.; Zubieta, J. *Polyhedron* **1987**, *6*, 1577−1585. (e) Nicholson, T.; Zubieta, J. *Polyhedron* **1988**, *7*, 171. (f) Nicholson, T.; Zubieta, J. *Inorg. Chem.* **1987**, *26*, 2093. (g) Nicholson, T.; Cook, J.; Davison, A.; Rose, D. J.; Maresca, K. P.; Zubieta, J.; Jones, A. G. *Inorg. Chim. Acta* **1996**, *252*, 421−426.

(37) (a) Baldas, J.; Bonnyman, J.; Willaims, G. A. *Inorg. Chem.* **1986**, *25*, 150−153. (b) Nicholson, T.; Zubieta, J. *Inorg. Chem.* **1987**, *26*, 2093.

Table 22. Comparison of Selected Bond Lengths[a] for **3**−**9** and **12** and Other Tc−Hydrazido and Re−Hydrazido Core Complexes[36]

	bond lengths (Å)					
	η^2-hydrazido			η^1-hydrazido		
chemical formula	M═N	N−N	M−N	M═N	N−N	ref
$[ReCl_3(NNC_5H_4NH)(HNNC_5H_4N)]$ (**3**)	1.934(9)	1.308(10)	2.165(7)	1.743(8)	1.249(12)	*b*
$[HNEt_3][ReCl_3(NNC_5H_4N)(HNNC_5H_4N)]$ (**4**)	1.940(13)	1.35(2)	2.170(14)	1.756(13)	1.25(2)	*b*
$[ReCl_3(NNC_3H_4N_2H)(HNNC_3H_4N_2)]$ (**5**)	1.977(24)	1.331(33)	2.073(7)	1.801(23)	1.272(74)	*b*
$[MoCl_3(NNC_5H_4NH)(HNNC_5H_4N)]$ (**6**)	1.960(8)	1.375(11)	2.237(7)	1.756(8)	1.266(11)	*b*
$[Tc(C_5H_4NS)_2(NNC_5H_4N)(HNNC_5H_4N)]$ (**7**)	1.985(9)	1.340(14)	2.150(7)	1.767(9)	1.237(13)	*b*
$[Re(C_5H_4NS)_2(NNC_5H_4N)(HNNC_5H_4N)]$ (**8**)	1.956(6)	1.323(10)	2.127(5)	1.766(6)	1.239(9)	*b*
$[Re(C_4H_3N_2S)_2(NNC_5H_4N)(HNNC_5H_4N)]$ (**9**)	1.966(28)	1.306(42)	2.096(20)	1.704(27)	1.279(39)	*b*
$[Mo(C_4H_3N_2S)_3(NNC_5H_4N)]$ (**12**)				1.794(4)	1.2396	*b*
$[ReCl_2(PPh_3)(NNC_5H_4N)(HNNC_5H_4N)]$	1.92(2)	1.34(3)		1.78(1)	1.21(2)	36a
$[Re(N_2COC_6H_5)(C_5H_4NS)Cl(PPh_3)_2]$				1.751(8)	1.270(11)	20
$[TcCl(PPh_3)_2(NNC_6H_4Br)_2]$				1.796(6) 1.783(7)	1.229(9) 1.224(8)	36b
$[TcCl_2(C_8H_5N_4)(PPh_3)_2]$				1.767(12)	1.274(17)	36c
$[Re(NNC_6H_4Br)_2(SC_6H_3-2,5\text{-}Me_2)(PPh_3)_2]$				1.730(13) 1.798(16)	1.324(17) 1.249(23)	36d
$[ReCl_2(PPh^3)(NNCOPh)]$	1.769(8)	1.30(2)				36e
$[Re(SNNS)(NNCOC_6H_4Cl)(PPh_3)]$[c]				1.76(2)	1.31(2)	36f
$[Re(SSSS)(NNCOPh)(PPh_3)_2]$[d]				1.76(2)	1.27(2)	36f

[a] Distances in Å. [b] This work. [c] (SNNS) = $\{SCH_2CH_2N(H)CH_2CH_2N(H)CH_2CH_2S\}^{2-}$. [d] (SSSS) = $\{SCH_2CH_2SCH_2CH_2SCH_2CH_2S\}^{2-}$.

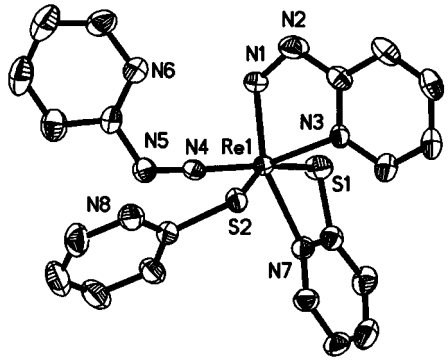

Figure 11. View of the structure of **8**, showing the atom-labeling scheme and 50% thermal ellipsoid probabilities.

in **5** correlates with the presence of the organohydraziniun-(1+) coordination mode of the chelating group.

The structures of compounds **7**−**9** are isomorphous and illustrate the consequences of substitution of the chloride ligands of the parent compounds **2**−**6** with pyridinethiol or pyrimidinethiol ligands. As illustrated in Figure 11 for the rhenium derivative $[Re(\eta^1\text{-}SC_5H_4N)(\eta^2\text{-}SC_5H_4N)(\eta^1\text{-}NNC_5H_4N)(\eta^2\text{-}HNNC_5H_4N)]$ (**8**), the compounds **7**−**9** adopt distorted octahedral geometry $\{ReS_2N_4\}$ defined by the sulfur donor of a pyridinethiol, the sulfur and nitrogen donors of a chelating pyridinethiol, the α-nitrogen of a monodentate pyridinediazenido(1−) ligand, and the α-nitrogen and the pyridyl nitrogen of a chelating pyridinediazene group. The metrical parameters associated with compounds **7**−**9** are quite similar and unexceptional in comparison to other metal−organohydrazino and metal−organothiolate complexes, as illustrated in Tables 22 and 23.

The X-ray diffraction study of **8** allows unambiguous assignment of the N1 position as the only nitrogen site bonded to a hydrogen. The $\{Re(NNC_5H_4N)(HNNC_5H_4N)\}$ core is thus identical to that of **4** and exhibits the anticipated orientation of the monodentate pyridinediazenido(1−) and the chelating pyridinediazene ligands. Compounds **7** and **9** exhibit this common core geometry. The occurrence of the identical ring conformation for the anionic organodiazenido(1−) groups relative to the bidentate organodiazene ligand in structures **4** and **7**−**9** suggests that this represents a favored geometry in the solid state, reflecting a combination of structural and steric contributions.

Table 23. Comparison of Metal−Sulfur Bond Lengths[a] of **7**−**9** and **12** with Those of Other Rhenium and Technetium Thiolate Species[37]

chemical formula	bond lengths: M−S (Å)	ref
$[Tc(C_5H_4NS)_2(NNC_5H_4N)(HNNC_5H_4N)]$ (**7**)	2.489(3)	*b*
$[Re(C_5H_4NS)_2(NNC_5H_4N)(HNNC_5H_4N)]$ (**8**)	2.477(2)	*b*
$[Re(C_4H_3N_2S)_2(NNC_5H_4N)(HNNC_5H_4N)]$ (**9**)	2.483(10)	*b*
$[Mo(C_4H_3N_2S)_3(HNNC_5H_4N)]$ (**12**)	2.482(1), 2.523(1), 2.530(1)	*b*
$[ReO(C_5H_4NS)_3]$	2.136(7), 2.242(6)	20
$[Re(N_2COC_6H_5)(C_5H_4NS)Cl(PPh_3)_2]$	2.476(3)	20
$[Re(PPh_3)_2(C_4H_3N_2S)_3]$	2.504(4), 2.497(6), 2.401(3)	20
$[TcN(C_9H_6NS)_2]$	2.3559(7)	37a
$[Re(SNNS)(NNCOC_6H_4Cl)(PPh_3)]$[c]	2.459(5), 2.348(5)	37b
$[Re(SSSS)(NNCOPh)(PPh_3)_2]$[d]	2.354(4), 2.483(5)	37b

[a] Distances in Å. [b] This work. [c] (SNNS) = $\{SCH_2CH_2N(H)CH_2CH_2N(H)CH_2CH_2S\}^{2-}$. [d] (SSSS) = $\{SCH_2CH_2SCH_2CH_2SCH_2CH_2S\}^{2-}$.

While the relative orientation of the pyridine and α-nitrogen atoms of the ligands suggests the possibility of hydrogen bonding between the ligands as the origin of this structural preference, the N6···H(N1) distance of 2.332 Å is inconsistent with significant hydrogen bonding between the sites.

The reaction of **6** with pyrimidinethiol was observed to yield a mixture of two compounds, one analyzing for $[Mo(SC_4H_3N_2)_2(NNC_5H_4N)(HNNHC_5H_4N)]$ (**11**) and a second minor component $[Mo(SC_4H_3N_2)_3(\eta^1\text{-}NNC_5H_4N)]$ (**12**). As shown in Figure 12, the structure of **12** consists of a distorted pentagonal bipyramidal core $\{MoS_3N_4\}$ with the pentagonal plane defined by the sulfur and nitrogen of two chelating pyrimidine ligands and the sulfur donor of the third chelating pyrimidinethiol, whose nitrogen donor occupies an axial site. The second axial site is occupied by the α-nitrogen of the pyridinediazenido-(1−) ligand. All ring hydrogens were observed in the final electron density maps, confirming that neither the pyrimidinethiol nitrogen sites nor the potential protonation sites of the pyridinediazenido(1−) ligand exhibit N−H bonding.

Seven-coordinate geometry is not unusual for Mo−organodiazenido species, having been previously observed for $[Mo(NNMe)(S_2CNMe_2)_3]$[32] and $[Mo(NNCO_2Et)(S_2CNMe_2)_3]$.[33] The metrical parameters associated with the $\{Mo(NNC_5H_4N)\}$ core of **12** are unexceptional, as illustrated in Table 22. The seven-coordinate rhenium−pyrimidinethiolate complex $[Re(PPh_3)$-

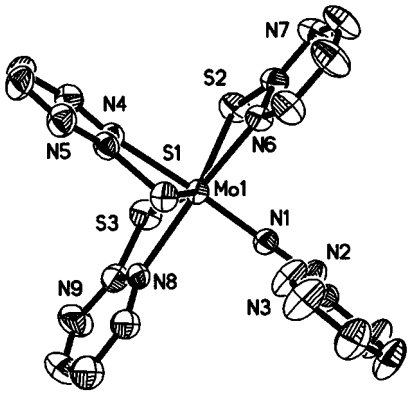

Figure 12. ORTEP view of the structure of **12**, showing the atom-labeling scheme and 50% thermal ellipsoid probabilities.

$(SC_4H_3N_2)_3]$[18] exhibits the same arrangement of chelating pyrimidinethiolate ligands and metrical parameters as those observed for the $\{MS_3N_3\}$ unit of **12**.

Conclusion

The ^{99m}Tc radionuclide has several advantages over other radionuclides which include cost, availability, and low-radiation-absorbed dose. The nuclear properties of ^{99m}Tc ($t_{1/2} = 6.02$ h; $\gamma = 146.6$ keV) enable rapid clinical evaluation. Radiopharmaceuticals utilizing rhenium, the group VIIB congener of technetium, in the form of the radioisotopes ^{186}Re and ^{188}Re, have been developed.[34] The nuclear properties of ^{186}Re are particularly attractive because of its half-life (90 h) and strong β emission ($\beta_{max} = 1070$ keV), which enable this isotope to deliver high radiation doses to tissues. Also, ^{186}Re has a photon emission at approximately the same energy as ^{99m}Tc ($\gamma = 137$ keV), allowing the radioisotope to be imaged by γ cameras utilized in conventional ^{99m}Tc diagnostic imaging. A rhenium radiopharmaceutical, ^{186}Re(Sn)HEDP has been developed for the palliation of painful osseus metastases.[35]

The periodic relationship between technetium and rhenium suggests that therapeutic technetium and rhenium radiopharmaceuticals will have similar biodistribution properties. Therefore, it is anticipated that ^{99m}Tc and ^{186,188}Re diagnostic agents which accumulate in abnormal tissue may be modeled with the development of analogues with existing cold rhenium agents.

The reaction of *N*-oxysuccinimidylhydrazinonicotinamide with chemotactic peptides possessing nucleophilic groups yields conjugates containing free hydrazine groups, HYNIC−peptide. These conjugates are readily labeled with ^{99m}Tc complexes to give {^{99m}Tc−(coligand)−HYNIC−peptide} complexes which are effective in the rapid detection of focal sites of infections in animals. While HYNIC-conjugated chemotactic peptides labeled with {^{99m}Tc-D-mannitol} gave impressive images, radio-HPLC indicated the presence of several {^{99m}Tc−(D-mannitol)−HYNIC−peptide} species. However, the addition of pyrimidine-2-thiol to the {^{99m}Tc−(D-mannitol)−HYNIC−peptide} resulted in ligand substitution to give a hydrophobic species {^{99m}Tc−(pyrimidine-2-thiol)−HYNIC−peptide} with modified biodistribution patterns compared to the mannitol derivative and other N,S-donor thiolate ligands.

In order to gain some insight into the fundamental coordination chemistry of the metal−HYNIC interaction and the subsequent ligand substitution by pyridinethiol and pyrimidinethiol, the reactions of various metal oxides $[MO_4]^{n-}$ (M = Tc, Re, Mo) with pyridylhydrazine in the presence of HCl were investigated, leading to the isolation of a series of complexes of general formulation $[MCl_3(\eta^1\text{-}NNC_5H_4NH_x)(\eta^2\text{-}HNNH_y\text{-}C_5H_4N)]$ ($x = 0$ or 1; $y = 0$ or 1). These complexes are stable in organic solvents and in mixed organic/aqueous media,[20] demonstrating the robust nature of metal−organohydrazine cores. However, the structural characterization of these compounds reveals a complex coordination chemistry, manifested in both monodentate terminal linkage and chelation by the organohydrazine ligands and by three distinct patterns for the relative orientations of the organohydrazine ligands in the $\{M(\eta^1\text{-}NNR)(\eta^2\text{-}HNNR)\}$ cores, which reflect the metal electronic requirements and the degree of ligand protonation. Thus, it is not surprising that the labeled protein conjugates are mixtures of materials as determined by radio-HPLC. While the coordination chemistry of the pyridylhydrazino ligand demonstrates the facility of complex formation and the robust nature of the complexes, it also suggests a variety of coordination modes for the radiopharmaceutical materials.

The parent complexes of the $[MCl_3(\eta^1\text{-}NNR)(\eta^2\text{-}HNNR)]$ class react smoothly with pyridinethiol and pyrimidinethiol to yield complexes of the class $[M(\eta^1\text{-}SRN)(\eta^2\text{-}SRN)(\eta^1\text{-}NNR)\text{-}(\eta^2\text{-}HNNR)]$. These latter compounds exhibit identical {metal−pyrdinediazenido(1−)−pyridinediazene} cores, indicating a simplified structural chemistry upon thiolate substitution. However, the detailed chemistry on the tracer level remains obscure, as the influence of the protein, the nature of the metal−HYNIC interaction, and the number and coordination modes of the pyridinethiol or pyrimidinethiol ligands are unknown. In order to address these issues, the coordination chemistry of Re and ^{99}Tc with selected HYNIC−peptide "ligands" and the influence of thiolates on such complexes are currently under investigation.

Acknowledgment. This work was supported by a grant from the Department of Energy Office of Health and Environmental Research (DE-FG02-93RG1571) to J.Z.

Supporting Information Available: Listings of crystal data, positional parameters, anisotropic thermal parameters, bond lengths and angles, and calculated hydrogen positions for **3**−**9** and **12** (50 pages). Ordering information is given on any current masthead page.

IC970352F